博士論文

Microfluidics-based analytical platform for nanoparticle characterization

(ナノ粒子の特性評価のための流体デバイスに基づく解析プラットフォーム)

マジャリカ ヴィレンドラ ジワンラオ

Microfluidics-based analytical platform for nanoparticle characterization

(ナノ粒子の特性評価のための流体デバイスに基づく解析プラットフォーム)

A thesis presented to the University of Tokyo

September, 2019

Majarikar Virendra Jiwanrao

Referee in chief: Professor Dr. Takanori Ichiki

Referee: Professor Dr. Madoka Takai

Referee: Associate Professor Dr. Hirotaka Ejima

Referee: Associate Professor Dr. Kanjiro Miyata

Referee: Associate Professor Dr. Horacio Cabral

TABLE of CONTENTS

CHAPTER 1

General introduction

CHAPTER 1 General introduction

1.1 Nanoparticle

Nanotechnology is one of the well-known scientific field dealing with the nanoscale-sized materials[1]. Nanoparticles (NPs) are diverse class of materials exhibiting the spherical, tubular or random shaped microscopic particles sized in nanometers[2] and display distinctive physical, optical and electrical properties[3]. Depending on the size, shape and properties, the various types of NPs were synthesized such as carbon-based NPs[4, 5], metal-based NPs[6], semiconductor-based NPs[7, 8], and polymer-based NPs[9, 10], etc. In addition, the synthesis of nanoparticle is divided into top-down and bottom-up approaches[11, 12] and it is very imperative to develop the synthesis method where nanoparticle have desirable and controlled characteristics. Here, top-down method involves the formation of nanoparticles by decreasing the size of the larger particles in a destructive approach whereas the bottom-up method starts with the simpler particles leading to the larger one. Moreover, the application of nanoparticle can range from the nanobiotechnology like targeted drug delivery, biomedical and pharmaceutical application[13-15] to the electronic and sensor[16, 17], owing to the unique properties of nanoparticles.

In this chapter, firstly in section 1.2, the general characterization techniques of nanoparticles are briefly reviewed, to show their underlying merits and demerits. Secondly, in section 1.3, the recent progress, on-going R&D and future prospect of

nanoparticle characterization is briefly described, to show that this thesis proposes to develop an analytical method for nanoparticle characterization by incorporating the unresolved issues. Thirdly, in section 1.4, the nanoparticle characterization in chip-based microcapillary electrophoresis (μCE) is described, to clarify the potential applicability of this device to characterize the biological nanoparticles. Later, in section 1.5, the underlying issues of the microcapillary electrophoresis chip are discussed. Then, in section 1.6, to solve the described issues in the microcapillary electrophoresis chip, the proposed research targets were introduced, and finally, section 1.7 provides the aim of this study, flow and structure of this thesis.

1.2 Nanoparticle measurement technology

The technology for characterization of nanoparticle varies greatly in principle and their development involve estimating the properties of nanomaterial. Traditionally, the characterization techniques of nanoparticles are used to estimate their structure, composition and properties, and are classified, but not limited, to optical, electron, scanning and photon-based methods[18]. Optical based characterization technique uses light scattering effect to determine the physical parameters, e.g. dynamic light scattering (DLS)[19] for particle sizing but multiple scattering, low resolution of size distribution histogram constitute its demerits. Electron based characterization technique such as scanning electron microscopy (SEM)[4, 20] and transmission electron microscopy (TEM)[21, 22] has high cost and time consuming, poor differentiability between nanoparticle and substrate, multiple steps for the image treatment represent their lacunae. Scanning probe e.g. atomic force microscopy (AFM)[23] used to characterize the topology and surface structure of the nanoparticles may be less expensive and time consuming but substrate roughness requires to be less than nanoparticle size. Subsequently, localized surface plasmon resonance (LSPR)[24] for nanoparticle analysis represent the photonic characterization technique. High sensitivity and automation represent their potential merits but lack differentiation of interactions with the sensor surface.

Moreover, a new characterization technique namely, nanoparticle tracking analysis (NTA) utilizing the properties of light scattering and Brownian motion to visualize and

analyze the NPs in liquid suspension based on Einstein-Stokes equation. Here, Brownian motion by the NPs relates to their size and distribution with diameter ranging from 10-nm to 1000-nm[25, 26]. The merits of this method involve the determination of the particle size and number whereas demerits represent the bad analysis result due to particle composed of materials with high refractive index, viscosity of the solvent, etc.

1.3 Nanoparticle characterization: on-going R&D and future prospect

The methodology for evaluation of nanoparticle (extracellular vesicles (EVs) including the exosomes) involve the principle and development for estimating the properties ranging from zeta potential to surface antigenicity. Evaluation of nanoparticle using the techniques, discussed in section 1.2, involve the major flaws where the demerits outweighs merits. In addition, a diverse range of particles, several tens to one hundred nanometers, make it extremely difficult to quantify, and hence, necessity to develop a new characterizing technique of nanomaterial[27].

Over the years, the technological application of lab-on-a-chip systems; developing the entire bio-chemical laboratory on the micron size polymer-based chips, is on the rise with ease of fabrication, minimum level of sample perturbation, greater simplicity, and more time efficient as potential merits[28, 29]. The chip-based microcapillary electrophoresis (μCE) is one of the characterization techniques of nanoparticles. Evaluation by microcapillary electrophoresis chip; consists of single microchannel fabricated using polydimethylsiloxane (PDMS) and glass substrate[30-32] with the application to measure the electrophoretic mobility (EPM) of nanoparticles based on the electroosmotic flow (EOF) in the microchannel of a μCE chip.

Recently, laser dark-field imaging has been employed to characterize the individual NPs using the μCE chip[33, 34]. Here, the visualization and measurement of individual NPs were achieved in a dark field within the microchannel of the microcapillary chip. NP detection takes place through the Rayleigh scattering of light of individual NPs in

the microchannel under the influence of electric field. Using the on-chip electrophoresis system, the imaging of individual exosomes in a dark field is possible by detecting laser light scattered from vesicles. In addition, researcher have demonstrated the zeta potential distribution of extracellular vesicles derived from the human breast cancer cells on chip-based immuno-electrophoresis[35, 36]. Here, the change in zeta potential due to the attachment of positively-charged antibodies on to the exosome's antigen represent the analysis of surface proteins.

The future prospect of nanoparticle characterization depend on the development of an analytical tool providing the range of NP properties within the single instrument[37]. These properties can be divided into, but not limited to:

(1) Ability to detect the individual nanoparticles with ease.

(2) Multiparametric profiling of nanoparticle within the single instrument e.g. size, concentration, zeta potential, etc.

(3) Target surface marker and dynamic state profiling between the nanoparticle and the biological membrane.

1.4 Microcapillary electrophoresis chip for nanoparticle characterization

One of the first applications of microfluidic device technology was a molecular analysis using chip-based microcapillary electrophoresis (μCE) in the early 1990s[38, 39]. Electrophoresis is an electrokinetic phenomena where charged particles undergo momentum relative to the fluid in presence of electric potential[40]. Moreover, the potential difference between the medium and stationary layers of the fluid attached to the particle disperse in the medium represents the zeta potential, whereas the electroosmotic flow is the electrolyte movement in an applied electric field in the fluid relative to a stationary charged surface[36, 41]. In comparison to other characterization techniques discussed earlier, evaluation by electrophoresis have minimum level of sample perturbation, greater simplicity, more time efficient, as potential merits. In addition, the significant advantages of the chip-based μCE technology are a reduction of the analysis time and sample volumes, the ease of electrokinetic fluid handling compared with electrophoresis using a silica capillary, and the compatibility of the integration of complex analytical procedures on a chip[42, 43]. Based on the research in the last few decades, the μCE technology has shown great potential, especially for the analysis and separation of biological samples, such as nucleotides, proteins, and living cells[44].

Electroosmotic flow in the microchannels of μCE chip is a laminar plug flow because of its low Reynolds number. This feature enables reliable measurements of

electrophoretic mobility, compared with traditional electrophoretic apparatus which involves turbulence flow. In recent years, there have been some remarkable studies on characterizing of biological nanoparticles using the chip-based microcapillary electrophoresis, particularly by laser dark-field imaging as discussed in section 1.3. Here, particle-by-particle measurement and visualization were achieved owing to the light scattered by nanoparticles under the influence of electric field. This μCE chip technology has been recognized as an important fundamental tool, especially for the characterization of extracellular vesicles[45]. The analysis of extracellular vesicles, including exosomes, can provide clinical information in diagnostics[46, 47].

The electrophoretic chip consists of microchannel fabricated using polydimethylsiloxane (PDMS) and glass substrate with two reservoirs, to determine the electrophoretic mobility of nanoparticles like exosomes. The microcapillary electrophoresis chip is consist of a microfluidic channel (length: 10 mm, width: 200 μm, height: 200 μm) and reservoirs (diameter: 5 mm) open at extreme ends as shown in Figure 1-1.

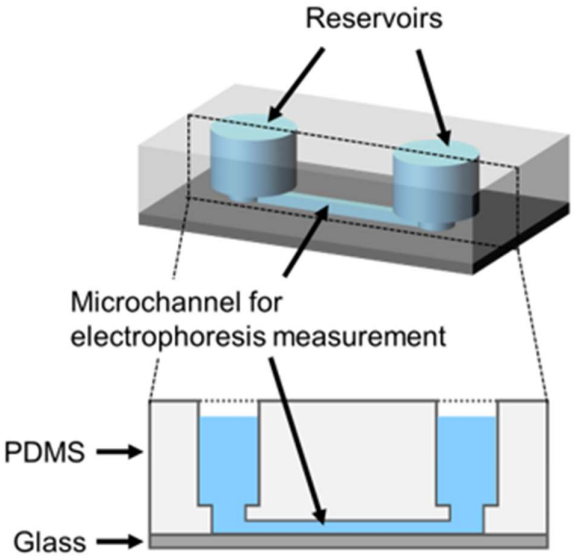

Figure 1-1 Schematic of a microcapillary electrophoresis (μCE) chip. The chip is consisting of a microfluidic channel (length: 10 mm, width: 200 μm, height: 200 μm) and reservoirs (diameter: 5 mm) open at top.

1.5 Issues in the microcapillary electrophoresis chip

Due to the microscale dimension of the microcapillary electrophoresis chip, there exist a number of undesirable issues which hinder the measurement of electrophoretic mobility of nanoparticles with ease. Thus, discussion about the issues in a microcapillary electrophoresis chip from the viewpoint of augmenting the analytical method for characterization of nanoparticles are required in order to develop an analysis platform for nanoparticles by extending the potential applicability of the chip. In general, the issues are the hydrodynamic issue arising from the height difference of fluid level between two reservoirs of microcapillary electrophoresis chip; electrochemical or Joule heating issue resulting due to the increase in the electrical conductivity and convection flow; and the adsorption issue of poly(dimethylpolysiloxane) (PDMS) based microchannel of a μCE chip.

1.5.1 Hydrodynamic issue

In the electrophoretic mobility measurement using a free-zone μCE chip, balancing the fluid level between the two reservoirs at the end of the microchannel is essential for avoiding the effect of the hydrostatic pressure flow. The hydrostatic pressure flow is unstable because of the small size of the microchannel, which is smaller than a single droplet of water. The height difference of the fluid level between the two reservoirs (inlet-side and outlet-side of the channel) induces hydrostatic pressure flow in the microchannel. Balancing the fluid level between the reservoirs can be easily achieved on a macroscale (e.g., > 10^{-3} m) by waiting for the disappearance of the hydrostatic pressure flow. However, on a microscale (e.g., 10^{-6}–10^{-3} m), the effect of the complexity of the interface dynamics appears as the instability of the hydrostatic pressure flow in the microchannel. Thus, when considering the μCE chip in the practical use, this balancing operation makes it difficult to measure the EPM with ease and accuracy in a short time due to the following reasons:

(i) The μCE chip requires a long time for balancing the fluid level between the two reservoirs because of the low fluid conductance of the microchannel.

(ii) The EOF in the microchannel produces an imbalance of the fluid height between the two reservoirs during measurement.

(iii) The instability of the meniscus in the reservoirs from the complexity of the interface dynamics induces perturbation of the hydrostatic pressure flow.

1.5.2 Electrochemical or Joule heating issue

The diameter of cylindrical shaped reservoirs in microcapillary electrophoresis chip is 3 mm open at the top. In the electrophoretic mobility measurement using a free-zone μCE chip, a gradual increase in voltage is required to determine the characteristics of the current and applied voltage (I-V) of fluids and electroosmotic flow velocity of nanoparticles. However, the presence of high voltage and use of low resistive solution in the small reservoirs lead to the unwanted issues. The application of high voltage and low resistivity solution during the measurement of electrophoretic mobility causes:

(i) Joule heating accompanies in the reservoirs with the mobility increase of the ions and generation of convection flow.

(ii) Change in the pH of fluid.

(iii) Formation of bubble at the electrodes by electrolysis.

1.5.3 Adsorption issue

The poly(dimethylsiloxane) (PDMS)-based microchannel of a microcapillary chip is attractive for characterization of nanoparticles[7-9]. However, the surface of native PDMS in the microchannels is negatively charged. Thus, when considering a PDMS-based microcapillary chip for practical use, this negative surface potential causes:

(i) Nanoparticle adsorption due to hydrophobic and/or electrostatic interaction.

(ii) Electroosmotic flow arising within the microchannel.

Hence, the surface properties of a PDMS-based microchannel demand further study to determine the nonspecific adsorption behavior of nanoparticles onto the surface of a microchannel, owing to the interaction between the particle and microchannel surface.

1.6 Research objectives

The measurement of EPM of nanoparticles using μCE chip can be achieved by addressing the individual issues separately. The hydrodynamic issue can be solved using the wider microchannel to improve the conductance of the microchannel whereas, for the electrochemical issue, limiting the electric current using the narrower microchannel and use of high-resistivity buffer solution to diminish the Joule heating effect. In addition, the adsorption issue can be solved by use of polymer coating on to the microchannel surface. However, it is impossible to solve the above conflicting issues by adjusting microchannel's dimension alone. Hence, to solve the number of undesirable issues in the microcapillary chip, we have proposed a new chip design by adding long-width bypass channel to balance the fluid level of two open-end reservoirs as shown in Figure 1-2. For this purpose, the research targets to be focused are:

1. Numerical simulation for laminar two-phase flow with phase field interface of μCE chip with the bypass channel to compensate the hydrostatic pressure flow in a microchannel.

2. Experimental evaluation of the compensation of the hydrostatic pressure and Joule heating in μCE chip with the bypass channel.

3. Adsorption phenomena of charged nanoparticles in presence of polymer as a coating agent on the microchannel in μCE chip with the bypass channel.

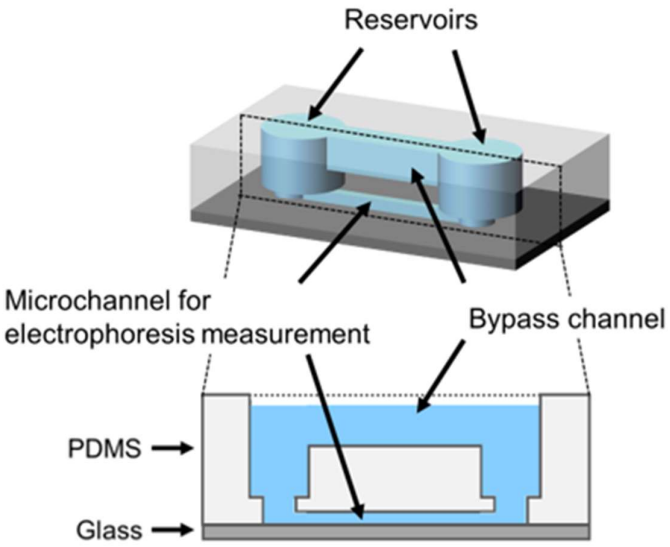

Figure 1-2 Schematic of a microcapillary electrophoresis (μCE) chip with the bypass channel. It consists of a microfluidic channel (length: 10 mm, width: 200 μm, height: 200 μm), reservoirs (diameter: 5 mm) and a bypass channel (length: 10 mm, width: 2 mm, height: 2 mm) open at top.

1.7 Aim of the study, flow and structure of the thesis

1.7.1 Aim of the study

The aim of this study is to develop an analysis platform for nanoparticles by extending the potential applicability of the microcapillary electrophoresis chip. To demonstrate the technological advancement in μCE chip with new design and the accuracy in electrophoretic measurement, the study of microcapillary electrophoresis chip technology includes four purposes as follows:

(1) Design and fabrication of microcapillary electrophoretic chip with long width bypass channel.

(2) Comparing the experimental and simulated results for electroosmotic flow (EOF) in newly fabricated chip.

(3) Analyze the adsorption behavior of charged nanoparticles in presence of polymer coated in microchannel.

(4) To determine the change in the zeta potential of nanoparticles during the enzymatic hydrolysis reaction as an application.

1.7.2 Flow of the thesis

Figure 1-3 show the flow of this thesis. It starts with the general introduction of nanoparticle and their characterization techniques in chapter 1. This thesis is divided into two main parts, namely, fundamental and application. In fundamental section, the issues in microcapillary chip was described in chapter 1. To solve the underlying issues, chapter 2 described the simulation of compensation of hydrostatic pressure in microcapillary chip with the bypass channel, chapter 3 described the experimental evaluation of compensation of hydrostatic pressure in microcapillary chip with the bypass channel and, lastly in chapter 4, the adsorption behavior of liposomes in presence of coated polymer in microcapillary chip with the bypass channel was discussed. Furthermore, in application section, chapter 5 show the temperature dependent adsorption behavior of nanoliposomes on PEG-modified surface. Finally, chapter 6 as general summary of the study.

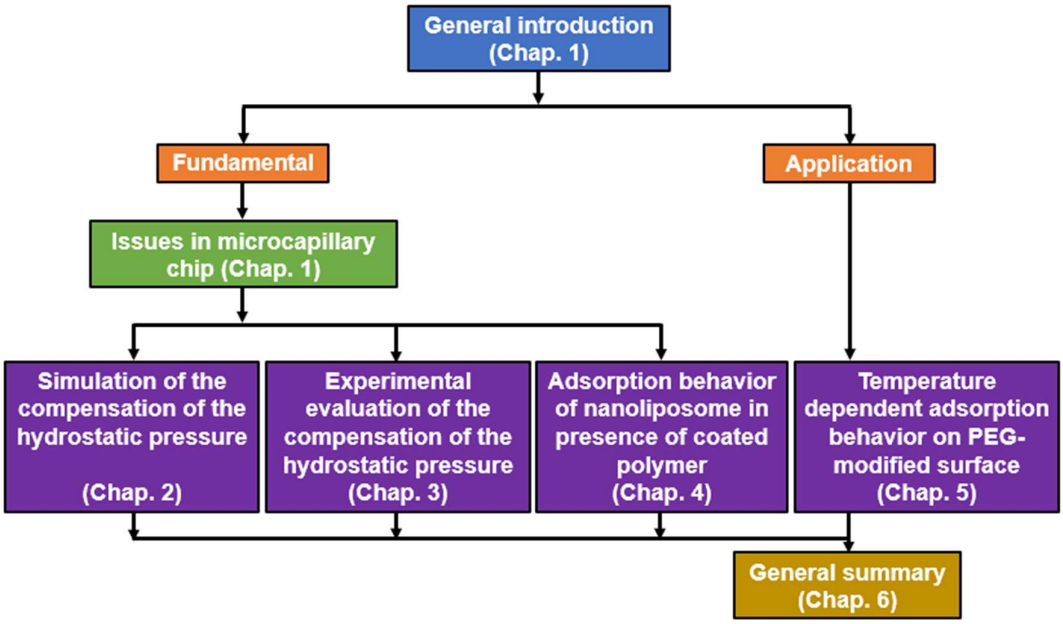

Figure 1-3 Flow of this thesis.

1.7.3 Structure of the thesis

This thesis proposes a new chip design by adding long-width bypass channel to balance the fluid level of two open-end reservoirs to solve the number of undesirable issues in the microcapillary electrophoresis chip. To develop an analysis platform for nanoparticles by extending the potential applicability of the microcapillary electrophoresis chip, (1) the introduction and underlying issues in a microcapillary electrophoresis chip for efficient measurement of EPM of nanoparticle, (2) simulation of compensation of hydrostatic pressure in microcapillary chip with the bypass channel, (3) evaluation of compensation of hydrostatic pressure in microcapillary chip with the bypass channel, (4) adsorption behavior of liposomes in presence of coated polymer in microcapillary chip with the bypass channel, and (5) temperature dependent adsorption behavior of nanoliposomes on PEG-modified surface were studied as shown in Figure 1-4. The thesis organizes general introduction, simulation of μCE chip with the bypass channel, evaluation of μCE chip with the bypass channel, adsorption behavior of liposomes, temperature dependent adsorption behavior on PEG, and general summary as follows.

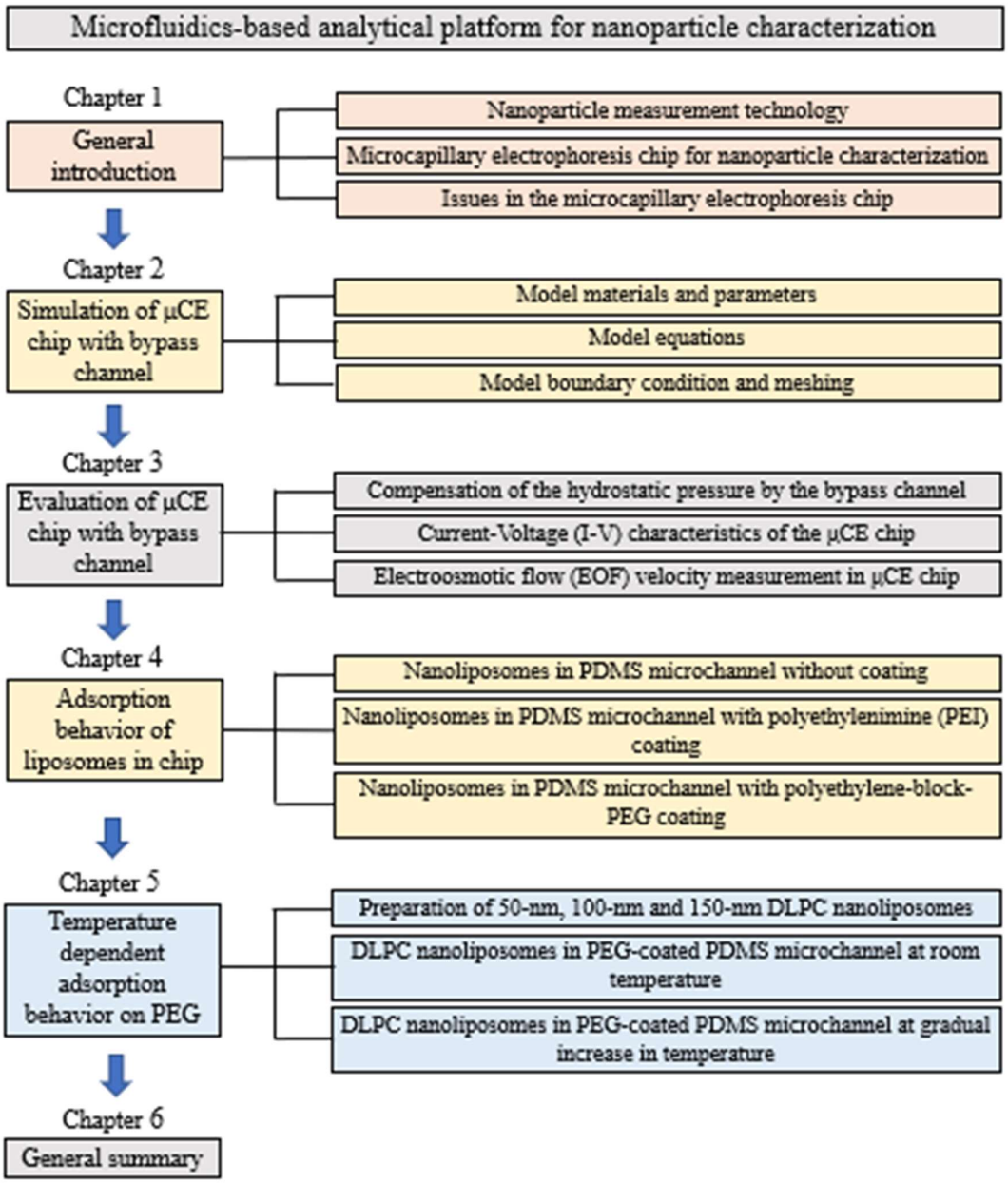

Figure 1-4 Structure of this thesis.

Chapter 1 provides the general introduction about the nanoparticles and the numerous characterization techniques with on-going R&D and future prospect. A new characterization method using the microcapillary electrophoresis chip for extracellular vesicles including the exosomes has been discussed. In addition, the detail overview of the issues in the microcapillary electrophoresis chip which hinders the accurate measurement of EPM of nanoparticle; and the proposed research targets to solve the issues in the chip were discussed. This thesis proposes to develop an analysis platform for nanoparticle by extending the potential applicability of the microcapillary electrophoresis chip.

Chapter 2 provides the overview of simulation of μCE chip with the bypass channel using the phase field method in COMSOL Multiphysics®. In section 2.2.1 and 2.2.2, the model materials and parameters selected to simulate the two-phase (air-water) interface using the phase field method are introduced. In section 2.2.3, the model equations required to couple with the dimension are discussed. Finally, in section 2.2.4, the selection and application of boundary conditions and meshing are introduced to simulate the chip-based 2D model for compensation of hydrostatic pressure flow and the inhibition of perturbation in the microchannel.

Chapter 3 provides the overview of experimental evaluation of the compensation of the hydrostatic pressure and Joule heating in μCE chip with the bypass channel. In section 3.2, the general steps to fabricate the chip with and without bypass channel and the experimental setup of laser dark-field imaging in the microchannel are described. In

section 3.3.1, compensation of the hydrostatic pressure in μCE chip with the bypass channel, and subsequent, comparison with chip without the bypass channel is introduced. In section 3.3.2, current-Voltage (I-V) characteristics of the μCE chip with and without the bypass channel is compared. Moreover, in section 3.3.3, measurement of electroosmotic flow in the chip with and without the bypass channel is discussed.

Chapter 4 provides the overview of cationic, anionic and neutral nanoliposomes exhibiting the adsorption behavior in μCE chip with the bypass channel in laser dark-field. Firstly, in section 4.2, materials and steps to prepare the nanoliposomes, characterization of PDMS-based microchannel coated with the neutral and cationic polymer, and dark-field imaging of nanoliposomes in the microchannel are discussed. In section 4.3.1, characterization of nanoliposomes via average size, average zeta potential, and concentration are described. Moreover, in section 4.3.2, characterization of the neutral and cationic polymer-coated PDMS microchannel with the 400-nm noncharged NPs is discussed. Finally, in section 4.3.3, adsorption behavior of nanoliposomes in PDMS microchannel without coating, with cationic polyethylenimine (PEI), and with neutral polyethylene-block-PEG coating are discussed.

Chapter 5 provides the overview of temperature dependent adsorption behavior of 50-nm, 100-nm, and 150-nm DLPC nanoliposomes on PEG-coated μCE chip with the bypass channel in laser dark-field. Firstly, in section 5.2, preparation of DLPC nanoliposomes, PDMS-based microchannel coated with the neutral PEG polymer, and dark-field imaging in the microchannel are briefly discussed. In section 5.3.1,

characterization of nanoliposomes via average size, average zeta potential, and concentration are described. Moreover, in section 5.3.2, DLPC nanoliposomes in PEG-coated PDMS microchannel at room temperature is discussed. Finally, in section 5.3.3, DLPC nanoliposomes in PEG-coated PDMS microchannel at gradual increase in temperature is discussed.

References

(1) R. P. Feynman: "There's plenty of room at the bottom" Engineering and Science, Vol. 22, pp. 22–36. (1960)

(2) S. Laurent, D. Forge, M. Port, A. Roch, C. Robic, L. Vander Elst, and R. N. Muller: "Magnetic iron oxide nanoparticles: synthesis, stabilization, vectorization, physicochemical characterizations, and biological applications" Chem. Rev., Vol. 110, pp. 2574–2574. (2010)

(3) M. Benelmekki: "An introduction to nanoparticles and nanotechnology" Designing Hybrid Nanoparticles, Morgan & Claypool Publisher (2015)

(4) K. Saeed, and I. Khan: "Preparation and characterization of single-walled carbon nanotube/nylon 6,6 nanocomposites" Instrum Sci. Technol., Vol. 44, pp. 435–444. (2016)

(5) K. Saeed, and I. Khan: "Preparation and properties of single-walled carbon nanotubes/poly(butylene terephthalate) nanocomposites" Iran. Polym. J., Vol. 23, pp. 53–58. (2014)

(6) E. C. Dreaden, A. M. Alkilany, X. Huang, C. J. Murphy, and M. A. El-Sayed: "The golden age: gold nanoparticles for biomedicine" Chem. Soc. Rev., Vol. 41, pp. 2740–2779. (2012)

(7) S. Ali, I. Khan, S. A. Khan, M. Sohail, R. Ahmed, A. Rehman, M. S. Ur Ansari, and M. A. Morsy: "Electrocatalytic performance of Ni@Pt core–shell nanoparticles supported on carbon nanotubes for methanol oxidation reaction" J. Electroanal. Chem., Vol. 795, pp. 17–25. (2017)

(8) T. Hisatomi, J. Kubota, and K. Domen: "Recent advances in semiconductors for photocatalytic and photoelectrochemical water splitting" Chem. Soc. Rev., Vol. 43, pp. 7520–7535. (2014)

(9) M. Mansha, I. Khan, N. Ullah, and A. Qurashi: "Synthesis, characterization and visible-light-driven photoelectrochemical hydrogen evolution reaction of carbazole-containing conjugated polymers" Int. J. Hydrogen Energy, Vol. 42, pp. 10952–10961. (2017)

(10) J. P. Rao, and K. E. Geckeler: "Polymer nanoparticles: preparation techniques and size-control parameters" Prog. Polym. Sci., Vol. 36, pp. 887–913. (2011)

(11) Y. Wang, and Y. Xia: "Bottom-up and top-down approaches to the synthesis of monodispersed spherical colloids of low melting-point metals" NanoLett., Vol. 4, pp. 2047–2050. (2004)

(12) S. Iravani: "Green synthesis of metal nanoparticles using plants" Green Chem., Vol. 13, pp. 2638–2650. (2011)

(13) J. Zhang, and M. Saltzman: "Engineering biodegradable nanoparticles for drug and gene delivery" Chem. Eng. Prog., Vol. 109, pp. 25–30. (2013)

(14) A. Loureiro, N. G. Azoia, A. C. Gomes, and A. Cavaco-Paulo: "Albumin-based nanodevices as drug carriers" Curr. Pharm. Des., Vol. 22, pp. 1371–1390. (2016)

(15) E. Martis, R. Badve, and M. Degwekar: "Nanotechnology based devices and applications in medicine: an overview" Chron. Young Sci., Vol. 3, pp. 68. (2012)

(16) M. Holzinger, A. Le Goff, and S. Cosnier: "Nanomaterials for biosensing applications: a review" Front. Chem., Vol. 2, 63. (2014)

(17) J. E. Millstone, D. F. J. Kavulak, C. H. Woo, T. W. Holcombe, E. J. Westling, A. L. Briseno, M. F. Toney, and J. M. J. Frechet: "Synthesis, properties, and electronic applications of size-controlled poly(3-hexylthiophene) nanoparticles" Langmuir, Vol. 26, pp. 13056–13061. (2010)

(18) M. Hassellöv, J. W. Readman, J. F. Ranville, and K. Tiede: "Nanoparticle analysis and characterization methodologies in environmental risk assessment of engineered nanoparticles" Ecotoxicology, Vol. 17, pp. 344–361. (2008)

(19) J. Lim, S. P. Yeap, H. X. Che, and S. C. Low: "Characterization of magnetic nanoparticle by dynamic light scattering" Nanoscale Research Letters, Vol. 8, 381. (2013)

(20) E. Mirzadeh, and K. Akhbari: "Synthesis of nanomaterials with desirable morphologies from metal–organic frameworks for various applications" Cryst. Eng. Comm., Vol. 18, pp. 7410–7424. (2016)

(21) N. Khlebtsov, and L. Dykman: "Biodistribution and toxicity of engineered gold nanoparticles: a review of in vitro and in vivo studies" Chem. Soc. Rev., Vol. 40, pp. 1647–1671. (2011)

(22) N. Khlebtsov, and L. Dykman: "Optical properties and biomedical applications of plasmonic nanoparticles" J. Quant. Spectrosc. Radiat. Transf., Vol. 111, pp. 1–35. (2010b)

(23) S. Fuentes, R. A. Zárate, E. Chávez, P. Muñoz, M. Ayala, R. Espinoza-González, and P. Leyton: "Synthesis and characterization of $BaTiO_3$ nanoparticles in oxygen atmosphere" Journal of Alloys and Compounds, Vol. 505, pp. 568–572. (2010)

(24) P. Singh: "LSPR Biosensing: Recent Advances and Approaches. In: Geddes C. (eds) Reviews in Plasmonics 2016" Reviews in Plasmonics, Vol. 2016. Springer,

Cham (2017)

(25) V. Filipe, A. Hawe, and W. Jiskoot: "Critical evaluation of nanoparticle tracking analysis (NTA) by nanosight for the measurement of nanoparticles and protein aggregates" Pharm. Res., Vol. 27, pp. 796–810. (2010)

(26) Y. Fan, P. Sahdev, L. J. Ochyl, J. J. Akerberg, and J. J. Moon: "Cationic liposome–hyaluronic acid hybrid nanoparticles for intranasal vaccination with subunit antigens" Journal of Controlled Release, Vol. 208, pp. 121–129. (2015)

(27) T. Akagi, and T. Ichiki: "Microcapillary Chip-Based Extracellular Vesicle Profiling System. In: Kuo W., Jia S. (eds) Extracellular Vesicles" Methods in Molecular Biology, Vol. 1660, Humana Press, New York (2017)

(28) T. Ichiki, T. Ujiie, S. Shinbashi, T. Okuda, and Y. Horiike: "Immunoelectrophoresis of red blood cells performed on microcapillary chips" Electrophoresis, Vol. 23, pp. 2029–2034. (2002)

(29) S. Kenyon, M. Meighan, and M. Hayes: "Recent developments in electrophoretic separations on microfluidic devices" Electrophoresis, Vol. 32, pp. 482–493. (2011)

(30) G. M. Whitesides: "The origins and the future of microfluidics" Nature, Vol. 442, pp. 368–373. (2006)

(31) D. Qin, Y. Xia, and G. M. Whitesides: "Soft lithography for micro- and nanoscale patterning" Nat. Protoc., Vol. 5, pp. 491–502. (2010)

(32) Y. Xia, and G. M. Whitesides: "Soft lithography" Annu. Rev. Mater. Sci., Vol. 28 pp. 153–184. (1998)

(33) K. Kato, M. Kobayashi, N. Hanamura, T. Akagi, N. Kosaka, T. Ochiya and T. Ichiki: “Electrokinetic evaluation of individual exosomes by on-chip microcapillary electrophoresis with laser dark-field microscopy” Jpn. J. Appl. Phys., Vol. 52, pp. 06GK10–1–06GK10–4. (2013)

(34) T. Akagi, N. Hanamura and T. Ichiki: “Measurement of individual nanobioparticles on microfluidic chips by laser dark-field imaging” J. Photopolymer Sci. Technol., Vol. 28, pp. 727–730 (2015)

(35) T. Ichiki, T. Ujiie, S. Shinbashi, T. Okuda, and Y. Horiike: "Immunoelectrophoresis of red blood cells performed on microcapillary chips" Electrophoresis, Vol. 23, pp. 2029–2034. (2002)

(36) T. Akagi, K. Kato, M. Kobayashi, N. Kosaka, T. Ochiya, and T. Ichiki: “On-chip immunoelectrohoresis of extracellular vesicles released from human breast cancer cells” PLoS ONE, Vol. 10, e0123603. (2015)

(37) D. L. M. Rupert, V. Claudio, C. Lässer, and M. Bally: "Methods for the physical characterization and quantification of extracellular vesicles in biological samples" Biochimica et Biophysica Acta, Vol. 1861, pp. 3164–3179. (2017)

(38) A. Manz, D. J. Harrison, E. M. J. Verpoorte, J. C. Fettinger, A. Paulus, H. Ludi, and H. M. Widmer: "Planar chips technology for miniaturization and integration of separation techniques into monitoring systems: Capillary electrophoresis on a chip" J. Chromatogr., Vol. 593, pp. 253–258. (1992)

(39) D. J. Harrison, K. Fluri, K. Seiler, Z. Fan, C. S. Effenhauser, and A. Manz: "Micromachining a miniaturized capillary electrophoresis-based chemical analysis system on a chip" Science, Vol. 261, pp. 895–897. (1993)

(40) C. C. Chang, and R. J. Yang: "Electrokinetic mixing in microfluidic systems" Microfluidics and Nanofluidics, Vol. 3, pp. 501–525. (2007)

(41) T. Akagi, K. Kato, N. Hanamura, M. Kobayashi, and T. Ichiki: "Evaluation of desialylation effect on zeta potential of extracellular vesicles secreted from human prostate cancer cells by on-chip microcapillary electrophoresis" Jpn. J. Appl. Phys., Vol. 53, 06JL01. (2014)

(42) T. Ichiki, Y. Sugiyama, and Y. Horiike: "Miniaturized capillary electrophoresis fabricated on pyrex glass chips using deep dry etching and anodic bonding" J. Photopolym. Sci. Technol., Vol. 15, pp. 311–316. (2002)

(43) A. Manz, and H. Becker: "Microsystem technology in chemistry and life sciences" Springer-Verlag Berlin Heidelberg, Berlin. (1998)

(44) R. Ashton, C. Padala, and R. S. Kane: "Microfluidic separation of DNA" Curr. Opin. Biotechnol., Vol. 14, pp. 497–504. (2003)

(45) S. Gholizadeh, M. S. Draz, M. Zarghooni, A. Sanati-Nezhad, S. Ghavami, H. Shafiee, and M. Akbari: "Microfluidic approaches for isolation, detection, and characterization of extracellular vesicles: current status and future directions" Biosens. Bioelectron., Vol. 91, pp. 588–605. (2017)

(46) D. Taylor, and T. C. Gercel: "MicroRNA signatures of tumor-derived exosomes as diagnostic biomarkers of ovarian cancer" Gynecologic oncology, Vol. 110, pp. 13–21. (2008)

(47) Y. Yoshioka, N. Kosaka, Y. Konishi, H. Ohta, H. Okamoto, H. Sonoda, R. Nonaka, H. Yamamoto, H. Ishii, M. Mori, K. Furuta, T. Nakajima, H. Hayashi, H. Sugisaki, H. Higashimoto, T. Kato, F. Takeshita, and T. Ochiya: "Ultra-sensitive liquid biopsy of circulating extracellular vesicles using ExoScreen" Nature communications, Vol. 5, pp. 3591. (2014)

CHAPTER 2

Simulation of microcapillary electrophoresis chip with the bypass channel

CHAPTER 2 Simulation of microcapillary electrophoresis chip with the bypass channel

2.1 Introduction

As discussed in previous chapter, microcapillary electrophoresis chip is used to measure the electrophoretic mobility for characterizing the nanoparticles. However, hydrostatic pressure flow in this chip render its ability to accurately determine the EPM. Hence, to solve this instability issue, we have designed a new chip by adding long-width bypass channel to balance the fluid level of two open-end reservoirs and remove the hydrostatic pressure flow within the microchannel as shown in Figure 1-2. The μCE chip is consist of a microfluidic channel (length: 10 mm, width: 200 μm, height: 200 μm) and reservoirs (diameter: 5 mm) open at extreme ends. In addition, the μCE chip with a bypass channel has an additional open channel (length: 10 mm, width: 2 mm, height: 2 mm). To test this new approach in chip design, the numerical modeling of fluid level adjustment for two immiscible fluids interface (air-water interface) with a bypass channel are simulated using the computational fluid dynamics (CFD) and microfluidic module within COMSOL Multiphysics®.

In this chapter, firstly in section 2.2, the simulation procedures for numerical modeling of fluid level adjustment for two immiscible fluids interface are briefly reviewed, to highlight the 2D model conditions and simulation workflow within the COMSOL Multiphysics®. In section 2.2.1, the model materials and, in section 2.2.2,

model parameters selected to simulate the two-phase interface are described. In section 2.2.3, the model equations required to couple with the dimension are discussed, to show the complexity and governing mechanism of phase field interface method. Moreover, in section 2.2.4, the selection and application of each boundary conditions and meshing coupled to the chip are introduced. Finally, in section 2.3, the obtained results for the numerical simulation of the electrophoresis chip with the bypass channel are discussed, to prove the assumption that adding a long-width bypass channel help to compensate the hydrostatic pressure flow in the microchannel.

2.2 Simulation procedure

Numerical modeling of fluid level adjustment for two immiscible fluids interface with a long-width bypass channel were simulated using computational fluid dynamics (CFD) and microfluidic module within COMSOL Multiphysics®[48]. Here, laminar fluid flow and phase field interface[49, 50] are coupled together to monitor the interface motion which is regulated by a Cahn-Hilliard equation[51-53]. Moreover, the coupled interface solves the Navier-Stokes equation for the fluid flow, a continuity equation, and transport equations involving the phase field variable, mixing energy density and free energy[54]. To simulate the fluid level balance, the simulation workflows within the software involve crafting the model dimension and appropriate geometry, assigning the physical parameters, material and meshing, and subsequently, selection of the phase initialization and time-dependent method.

2.2.1 Model materials

Numerical simulation of two-phase (air-water) interface using the phase field method involve the coupling of materials to the cross-sectional dimension of the μCE chip consisting of microchannel, bypass channel, and two reservoirs. Table 2-1 show the data on the materials content selected to simulate the fluid interface. In addition, Figure 2-1 shows the 2D model of μCE chip with the bypass channel with the coupled model materials.

Table 2-1 Data on model materials content

Property	Air	Water
Relative Permittivity	1	80
Dynamic Viscosity	1.81×10^{-5} [Pa.s]	1×10^{-3} [Pa.s]
Electrical Conductivity	0 [S/m]	5.5×10^{-6} [S/m]
Density	1.225 [kg/m^3]	997 [kg/m^3]

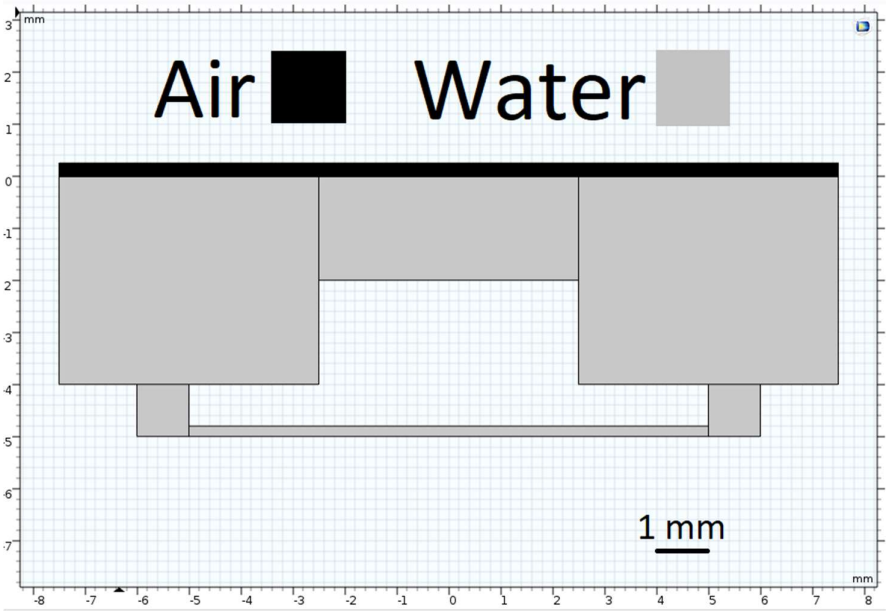

Figure 2-1 COMSOL 2D model of μCE chip with the bypass channel with the coupled air and water material.

2.2.2 Model parameters

Table 2-2 show the information on the model parameters selected to simulate the two-phase (air-water) interface using the phase field method of μCE chip with the bypass channel.

Table 2-2 Data on model parameters

Symbol	Expression	Description
ζ	-30 [mV]	Zeta potential of the fluid
E	0 [V] and 5 [V]	Applied electric potential
ε_{pf}	6.5×10^{-5} [m]	Parameter controlling interface thickness
χ or γ	1 [m.s/kg]	Mobility tuning parameter
$\partial f/\partial \emptyset$	1 [J/m^3]	Phi-derivative of external free energy
θ_w	Water: 1.939 [rad]	Contact angle of the fluid with PDMS
σ	Water: 0.07199 [N/m]	Surface tension coefficient with air
Ψ	1	Phase field help variable
λ	0.5×10^{-6} [N]	Mixing energy density
$\emptyset$	-1 to 1	Phase field variable

2.2.3 Model equations

Numerical simulation of fluid interface tracking using the phase field method and electroosmotic flow involves the physics equations[54]:

(a) Navier-Stokes equation for incompressible flow describing the flow in the channel

$$\rho(u \cdot \nabla)u = \nabla \cdot [-pI + \mu(\nabla u + (\nabla u)^T] + F$$

$$\rho \nabla \cdot (u) = 0$$

Where pI is pressure gradient, ρ is density of fluid, μ is viscosity of fluid, F is external force and u is fluid velocity.

(b) Helmholtz-Smoluchowski for electroosmotic velocity and the electric field strength

$$u = \mu_{eo} E_t \,, \quad \mu_{eo} = -\frac{\varepsilon_r \varepsilon_0 \zeta}{\mu} \,, \quad E_t = E - (E \cdot n)n$$

Where ζ is zeta potential of the fluid, E is applied electric potential, E_t is electric field strength, ε_0 is permittivity of vacuum, ε_r is dielectric constant of fluid, μ is viscosity of fluid and μ_{eo} is electrophoretic mobility.

(c) Phase field

$$\frac{\partial \emptyset}{\partial t} + u \cdot \nabla \emptyset = \nabla \cdot \frac{\gamma \lambda}{\varepsilon^2} \nabla \Psi \,, \qquad \emptyset = phipf$$

$$\Psi = -\nabla \cdot \nabla \emptyset + (\emptyset^2 - 1)\emptyset + \frac{\varepsilon^2}{\lambda} \frac{\partial f}{\partial \emptyset} \,, \quad \Psi = psi$$

$$\lambda = 3\varepsilon_{pf}\sigma/\sqrt{8}\,,\ \ \gamma = \chi$$

Where λ is mixing energy density, ε_{pf} is parameter controlling interface thickness, χ or γ is mobility tuning parameter, $\frac{\partial f}{\partial \emptyset}$ is phi-derivative of external free energy, σ is surface tension coefficient with air and $\emptyset$ is phase field variable.

(d) Cahn-Hilliard equation for diffuse interface immiscible phase

$$F_{st} = \left(\frac{\lambda}{\varepsilon_{pf}^2}\Psi - \frac{\partial f}{\partial \emptyset}\right)\nabla\emptyset$$

$$\rho = \rho_1 V_{f1} + \rho_2 V_{f2} \quad , \quad \mu = \mu_1 V_{f1} + \mu_2 V_{f2}$$

$$V_{f1} = \frac{1-\emptyset}{2}\ ,\ V_{f2} = \frac{1+\emptyset}{2}\ ,\ V_{f1} + V_{f2} = 1$$

Where $\emptyset$ is phase field variable, Ψ is phase field help variable and V_f is volume fraction.

(e) Wetted Wall

$$n \cdot \frac{\gamma\lambda}{\varepsilon^2}\nabla\Psi = 0$$

$$n \cdot \nabla\emptyset = \cos(\theta_w)\,|\nabla\emptyset|$$

Where θ_w represent the contact angle of the fluid with PDMS.

2.2.4 Model boundary conditions and meshing

Electroosmotic velocity was applied to two horizontal channels with built-in expression for electroosmotic mobility and zeta potential of -30 [mV]. A no-slip boundary condition with an open boundary at the top and an electric potential of 0 [V] and 5 [V] on the left and right electrodes, respectively, were used as shown in Figure 2-2. A wetted wall with a contact angle and surface tension coefficient with the fluid-gas interface were applied as 1.939 rad and 0.07199 N/m, respectively. To model mesh, mapped meshing with maximum and minimum element size of 0.13 mm and 0.0015 mm respectively, were coupled as shown in Figure 2-3.

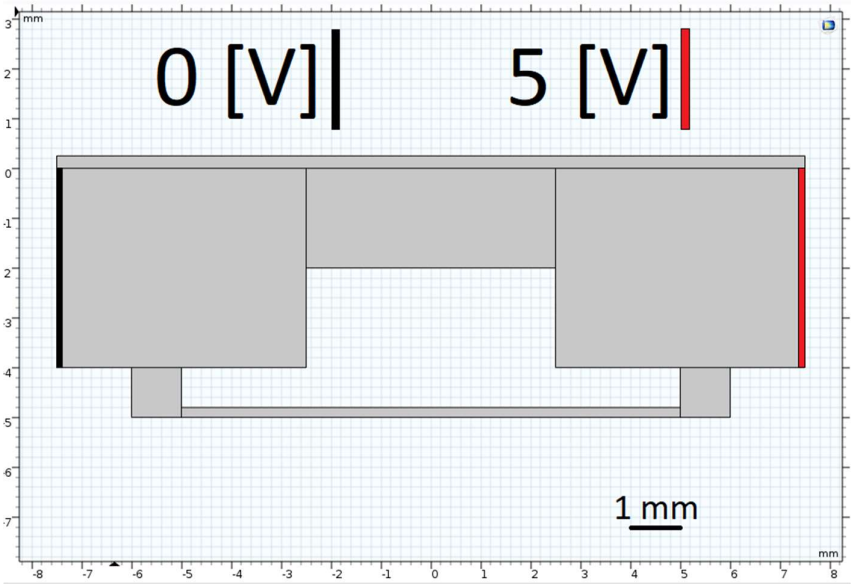

Figure 2-2 COMSOL 2D model of μCE chip with the bypass channel depicting the left and right electrodes position.

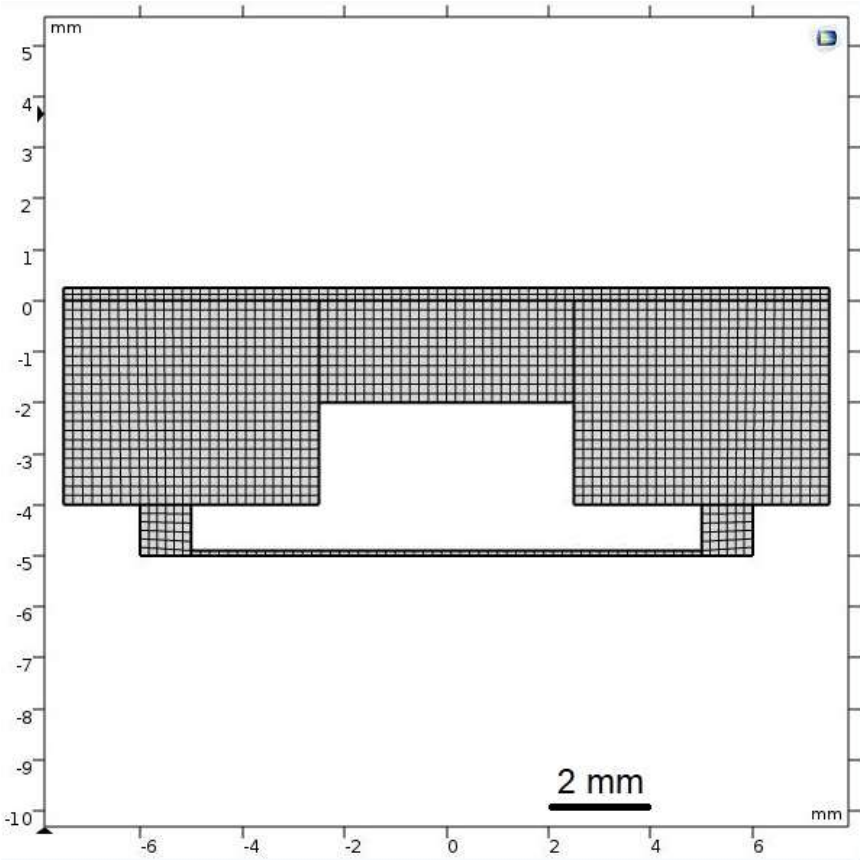

Figure 2-3 COMSOL 2D model of μCE chip with the bypass channel depicting the mapped meshing.

2.3 Results and discussion

Numerical simulation of the laminar two-phase flow with the phase field interface (air-water interface) depicting the 2D cross-sectional dimension of the electrophoresis chip include the microchannel, bypass channel, and two reservoirs. A new chip was designed by adding long-width bypass channel to balance the fluid level of two open-end reservoirs and show the following results:

(a) Volume fraction of fluid with the air-water interface

The shape of the air-water interface was flat and the contact angle was observed at the air-water-wall interface as shown in Figure 2-4(a).

(b) Distribution of the fluid velocity at the applied voltage of 5 V

The velocity flow in one direction at the microchannel is arisen from the electro osmotic flow with the applied voltage 5 V as shown in Figure 2-4(b).

The 2D simulation of electrophoresis chip with the bypass channel qualitatively show two important physical essences of:

(i) Compensation of hydrostatic pressure flow

(ii) Inhibition of perturbation in the microchannel

The result of 2D simulation provide the sufficient information about the role of the bypass channel to remove the hydrostatic pressure flow in the microchannel.

(a)

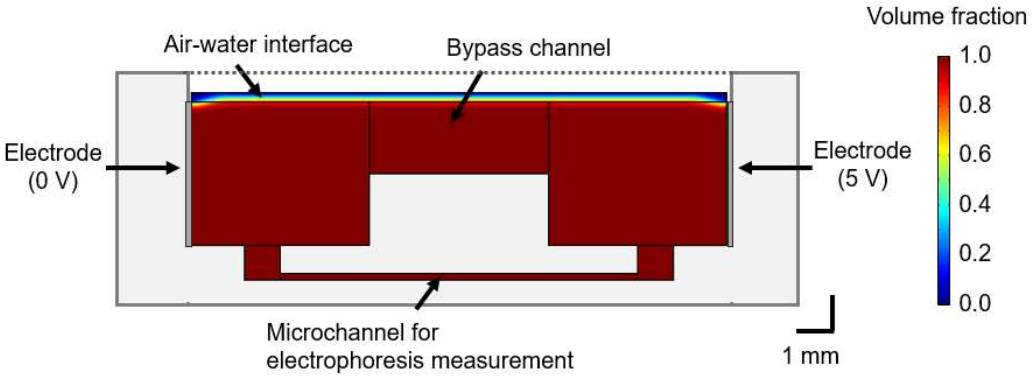

(b)

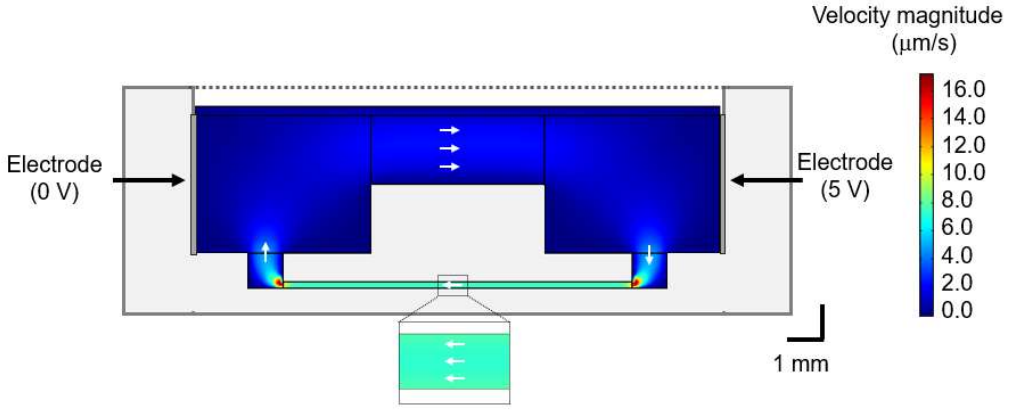

Figure 2-4 Numerical simulation of the laminar two-phase flow with the phase field interface (air-water interface) for the electrophoresis chip with the bypass channel. (a) The volume fraction of fluid with the air-water interface. (b) The distribution of the fluid velocity in the electrophoretic chip with the bypass channel in the presence of the applied electric potential of 5 V.

2.4 Summary of this chapter

In this chapter, numerical modeling of fluid level adjustment for air-water interface with laminar fluid flow and phase field interface in microcapillary chip with a bypass channel using the computational fluid dynamics and microfluidic module within COMSOL Multiphysics® were introduced.

In section 2.2.1, model materials selected to simulate the two-phase interface in μCE chip with the bypass channel were introduced. Here, the properties of air and water such as relative permittivity, dynamic viscosity, density and electrical conductivity were selected and coupled to the domains of the cross-sectional dimension of the μCE chip with the bypass channel.

In section 2.2.2, model parameters selected to simulate the two-phase interface in μCE chip with the bypass channel were described. Here, the range of model parameters such as zeta potential of the fluid, applied electric potential of 0 V and 5 V, parameter controlling interface thickness and mobility tuning, and phase field variables governing the numerical simulation of air-water interface were coupled with the model. In addition, contact angle of the fluid with PDMS and surface tension coefficient with air were selected to estimate the shape of the air-water-wall interface.

In section 2.2.3, the selection of equations to simulate the two-phase interface in μCE chip with the bypass channel were introduced. The equations coupled with the 2D model were Navier-Stokes equation for the flow in the channel, electroosmotic velocity and the electric field strength governing by Helmholtz-Smoluchowski, air-water interface motion

regulated by Cahn-Hilliard equation and phase field, and contact angle of air-water-wall by wetted wall.

In section 2.2.4, the selection of model boundary conditions and meshing coupled to the μCE chip with the bypass channel were introduced. Here, two horizontal channels were coupled for electroosmotic mobility and zeta potential of -30 [mV], an electric potential of 0 V and 5 V on the left and right side of the chip wall as electrodes, wetted wall with a contact angle and surface tension coefficient with the fluid-gas interface were applied.

In section 2.3, the obtained results for the numerical simulation of the μCE chip with the bypass channel were discussed. Here, the volume fraction of fluid and fluid velocity distribution in the μCE chip with the bypass channel in the presence of the applied electric potential of 5 V show the compensation of hydrostatic pressure flow and inhibition of perturbation in the microchannel. Hence, proving the assumption that addition of long-width bypass channel help to compensate the hydrostatic pressure flow in the microchannel.

References

(48) COMSOL Multiphysics, ver. 5.2a, www.comsol.com (2016)

(49) Capillary Filling - Phase Field Method: https://www.comsol.jp/model/capillary-filling-8212-phase-field-method-1878

(50) N. Takada, M. Misawa, and A. Tomiyama: "A Phase-Field Method for Interface-Tracking Simulation of Two-Phase Flows" Mathematics and Computers in Simulation, Vol. 72, pp. 220–226. (2006)

(51) E. Olsson, and G. Kreiss: "A conservative level set method for two phase flow" J. Comput. Phys., Vol. 210, pp. 225–246. (2005)

(52) N. Takada, and A. Tomiyama: "A Numerical Method for Two-Phase Flow Based on a Phase-Field Model" JSME International Journal Series B - Fluids and Thermal Engineering, Vol. 49, pp. 636–644. (2006)

(53) F. O. Alpak, B. Riviere, and F. Frank: "A phase-field method for the direct simulation of two-phase flows in pore-scale media using a non-equilibrium wetting boundary condition" Comput. Geosci., Vol. 20, pp. 881–908. (2016)

(54) CFD Module User Guide, ver. 5.0, Comsol. (2015)

CHAPTER 3

Experimental evaluation of microcapillary electrophoresis chip with the bypass channel

CHAPTER 3 Experimental evaluation of microcapillary electrophoresis chip with the bypass channel

3.1 Introduction

In chapters 1 and 2, the issues in the microcapillary electrophoresis chip causing the hinderance for the accurate measurement of EPM of nanoparticle and simulation of μCE chip with the bypass channel in COMSOL Multiphysics® as one of the proposed research targets were introduced. Chapter 3 introduces the experimental evaluation of the compensation of the hydrostatic pressure and Joule heating in μCE chip with the bypass channel. As demonstrated by simulation, the presence of extra bypass channel in microcapillary electrophoresis chip balance the fluid level of two open-end reservoirs and remove the hydrostatic pressure flow within the microchannel, and thereby, facilitating the evaluation of EPM with ease. To compare the simulated EPM of nanoparticle with that of the experimental, μCE chip with and without the bypass channel are fabricated and individual NPs measurement are achieved by laser dark-field imaging.

Firstly, in section 3.2.1, the general steps to fabricate the microcapillary chip with and without the bypass channel is introduced. Secondly, in section 3.2.2, the experimental setup and principle of laser dark-field imaging in the microchannel is described, to show the effectiveness in individual nanoparticle detection. Then, in section 3.3.1, compensation of the hydrostatic pressure in μCE chip with the bypass

channel, and subsequent, comparison with μCE chip without the bypass channel are described, to clarify the advantage of long-width bypass channel in compensating the hydrostatic pressure flow. In section 3.3.2, current-Voltage (I-V) characteristics of the μCE chip with and without the bypass channel is compared, to demonstrate the inhibition of Joule heating in chip. Finally, in section 3.3.3, measurement of electroosmotic flow in the chip with and without the bypass channel is discussed, to show that there is no remarkable difference in EOF velocity values between the μCE chips.

3.2 Experimental procedure

3.2.1 Fabrication of on-chip μCE with and without bypass channel

The microcapillary electrophoresis chip made up of poly(dimethylpolysiloxane) (PDMS) and glass substrate was fabricated by soft lithography [30-32]. Briefly, the fabrication steps involve the photo resist deposition on to the silicon wafer, photo mask and UV light exposure for designated time and temperature, mask remover and photoresist dissolution with PDMS and curing agent treatment, and subsequent peel off the PDMS slab with micropatterned embossed in it. The dimension of μCE chip with and without the bypass channel were exactly same as mentioned in the introduction of numerical simulation of μCE chip on chapter 2.

3.2.2 Laser dark-field imaging in the microchannel

An experimental setup of the on-chip μCE chip with a laser dark-field imaging were consists of a μCE chip, a high voltage dc power supply, a pair of platinum electrodes, a 405-nm laser source, an inverted microscope, and an sCMOS camera. Detection of nanoparticles (NPs) was based on dark field imaging of the laser light scattered by the NPs under its vicinity. A 405-nm light was focused on the microchannel filled with a NP suspension. An electric field was applied across two vertical arms with varied potential ranging from 0 to 50 V. The NPs under the influence of the potential moved along the microchannel (200 μm in width, 200 μm in height, and 10 mm in length). A Rayleigh scattering image of the NPs in the microchannel was simultaneously captured via the sCMOS camera as shown in Figure 3-1. Non-charged nanoparticles (Non-charged NPs) which are polystyrene particles with a 400-nm diameter coated with hydroxyl propyl cellulose were dissolved in water and PBS. Sample solution was loaded into the microchannel of the μCE chip, as follows. First, sample solution was pipetted into the left reservoir of the μCE chip. Subsequently, it was introduced into the microchannel by suctioning from the right reservoir using a syringe. Then, the bypass channel and the reservoirs were filled with the sample solution.

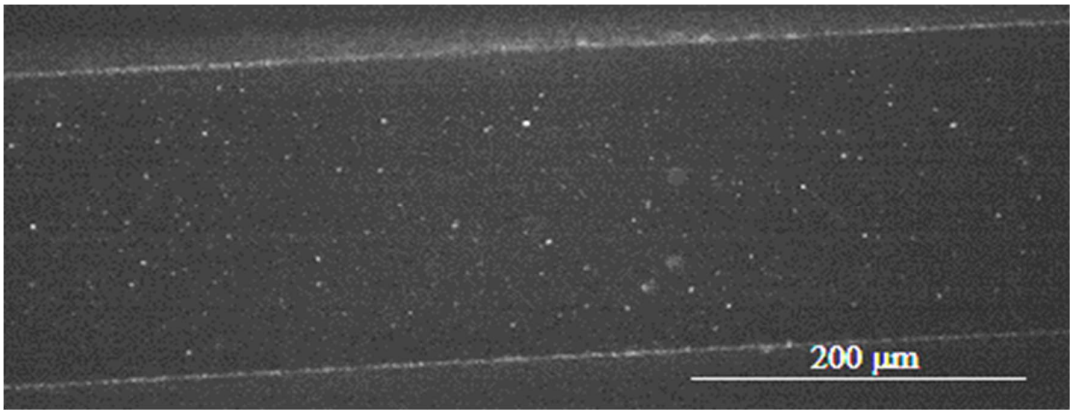

Figure 3-1 sCMOS image of 400 nm non-charged polystyrene nanoparticles in milli-Q water in laser dark-field imaging in the microchannel of μCE chip with the bypass channel.

3.3 Results and discussion

3.3.1 Compensation of the hydrostatic pressure by the bypass channel

The compensation of the hydrostatic pressure in μCE chip with the bypass channel were preformed experimentally, and compared with the μCE chip without the bypass channel, as there was a structural difference between the two fabricated μCE chips. Firstly, the hydrostatic pressure compensation of the bypass channel that was designed to improve the stability of the fluid flow in the microchannel was evaluated. To test this fluid flow stability, images of the position of the polystyrene NPs in the microchannel for the μCE chips with and without the bypass channel, were captured between 0 and 30 min. A 1-μL droplet of the NP suspension was added at 1 min in one of the reservoirs to produce a hydrostatic pressure from the height difference between the reservoirs. As shown in Figure 3-2, the NPs in the microchannel of the μCE chip without the bypass channel flowed by the hydrostatic pressure flow owing to the disruption of the fluid equilibrium levels at their reservoir. With the addition of a small volume of the droplet of 1 μL, a long balancing time of the fluid level was required, because of the low fluid conductance of the narrow microchannel. The behavior of fluids flowing in the microchannel of μCE chip follows a Poiseuille flow; steady-state fluid flow induced by pressure difference in a long straight channel. The volume flow rate Q in the microchannel could be theoretically predicted from the applied hydrostatic pressure ΔP and the microchannel resistance R[55, 56].

$$Q = \frac{\Delta P}{R}$$

From the Navier–Stokes equations, the microfluidic resistance of a square cross-sectional microchannel R is expressed as shown below[57]

$$R = \frac{12\eta L}{1 - 0.917 \times 0.63} \frac{1}{h^4}$$

The parameter η is the viscosity of the liquid, 0.001 Pa·s, and L is the microchannel length, 10 mm. The parameter h is the width and height of the square microchannel, 200 μm. The hydrostatic pressure created from the difference of the fluid level between the two reservoirs h is given as

$$\Delta P = \rho g h$$

The parameter ρ is the density of the liquid, 997 kg/m^3, and g is the gravity acceleration, 9.8 m/s^2. The average velocity in the microchannel was calculated from the volume flow rate Q and the cross-sectional area of the microchannel. The theoretically predicted temporal change in the velocity after the addition of the 1-μL droplet is shown in Figure 3-2, and the balancing time was estimated to be approximately 5 min.

Surprisingly, the fluctuation of the fluid velocity was still observed over the balancing time of the height difference of the fluid level between the two reservoirs. The meniscus instability at the fluid-wall interface resulted in the fluid velocity fluctuation

over the balancing time. This instability of the meniscus is known as the **Saffman-Taylor-like instability**[58-60]. Saffman-Taylor instability (also known as viscous fingering or Hele-Shaw flow) arises when a fluid is pushed on to a more viscous fluid between closely spaced parallel plates. The interface between the fluids develops a hydrodynamic instability leading to the formation of finger-like patterns. The μCE chip with the bypass channel compensated this fluid imbalance with minimal movement of the NPs in the microchannel (only a Brownian motion was observed), as shown in Figure 3-3. These results indicated that the bypass channel eliminated the generation of an unstable hydrostatic pressure flow in the microchannel by compensating the fluctuation of the hydrostatic pressure created from the instability of the meniscus in the reservoirs.

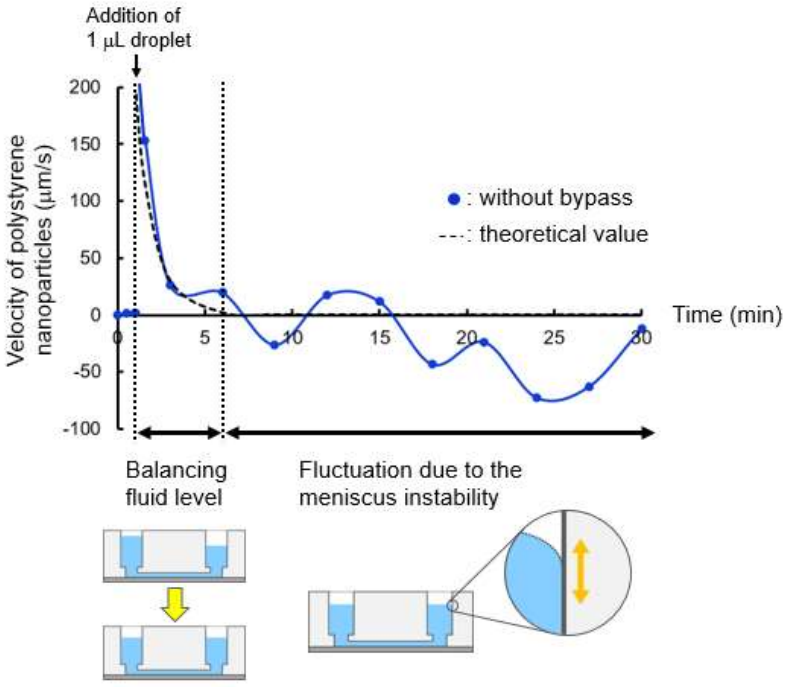

Figure 3-2 The temporal velocity changes of the polystyrene NPs in the microchannel of the μCE chip without the bypass channel. The fluctuation of the fluid flow created from the instability of the meniscus at the water-wall interface in the reservoirs was observed over the balancing time of the fluid level.

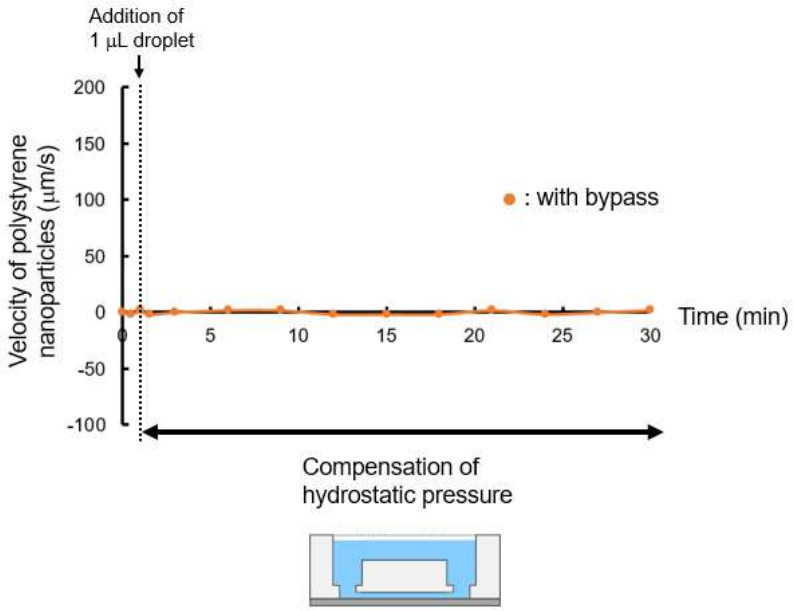

Figure 3-3 The temporal velocity changes of the polystyrene NPs in the microchannel of the μCE chip with the bypass channel. The presence of bypass channel causes the compensation of the hydrostatic pressure, and the fluid flow in the microchannel in the μCE with the bypass channel was stable even with the addition of the 1-μL droplet.

3.3.2 Current-Voltage (I-V) characteristics of the μCE chip with and without the bypass channel

The characteristics of the current and applied voltage (I-V) for water, HEPES (4-(2-hydroxyethyl)-1-piperazineethanesulfonic acid) buffer, and phosphate buffered saline (PBS) in the two fabricated μCE chips with and without the bypass channel represented in Figures 3-4 and 3-5 respectively. The I-V characteristics followed Ohm's law. Considering the Ohm's law, current I can be determined from the applied voltage V and the electric resistivity R. The R of a microchannel can be calculated as $R = l/(C \times A)$, where C is the conductivity of the solution, l is the length of the microchannel, and A is the cross-sectional area. Thus, the difference in current between the μCE chip with and without the bypass channel is due to the difference between the cross-sectional areas and the difference between the conductivities of the solution. The measured current in the μCE chip with the bypass was approximately $0.8–1.0 \times 10^2$ times higher than that of the μCE chip without the bypass channel, because the additional large channel facilitated more ion movement. Moreover, the measured current for PBS was high owing to its higher electrical conductivity and ionic strength than that of water. In addition, for PBS in the μCE chip with the bypass channel, a further increase of the I-V characteristics resulted in a deviation from linearity over 10 V. This deviation could be considered from the effect of Joule heating accompanied with the mobility increase of the ions[42].

(a)

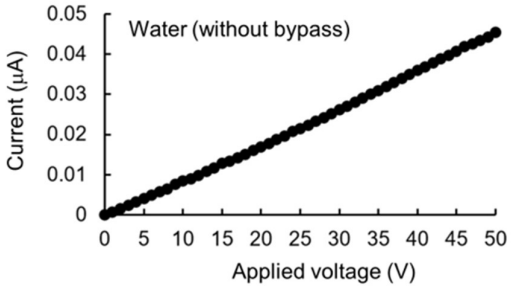

(b)

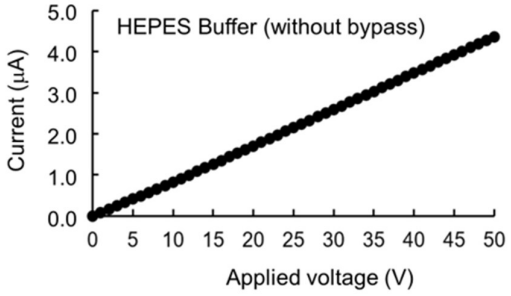

(c)

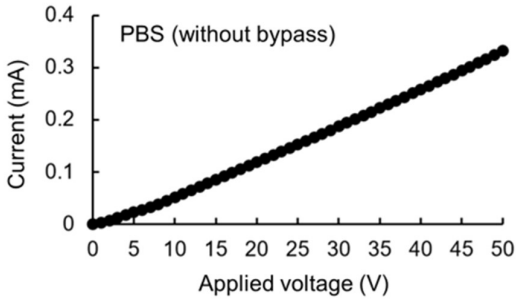

Figure 3-4 Plot of the current and applied voltage for (a) water, (b) HEPES buffer, and (c) PBS in the μCE chip without the bypass channel.

(a)

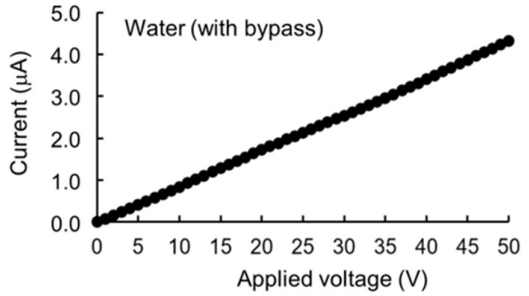

(b)

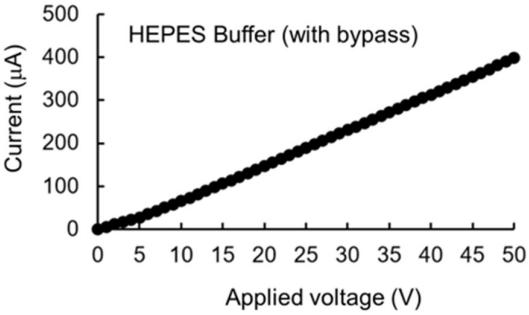

(c)

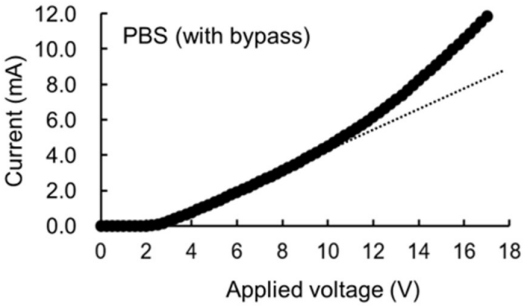

Figure 3-5 Plot of the current and applied voltage for (a) water, (b) HEPES buffer, and (c) PBS in the μCE chip with the bypass channel. The bypass channel enabled more ion movement within its dimension, and thereby, produced a multiple fold increase in the measured current for the different solution than that of the chip without the bypass channel. The deviation from linearity owing to the mobility increase created from Joule heating was observed in the electrophoresis chip with the bypass channel for PBS.

3.3.3 Electroosmotic flow (EOF) velocity measurement in the μCE chip with and without the bypass channel

Figures 3-6 show the plots of the migration velocity of the non-charged NPs and applied voltage for μCE chips without and with the bypass channel. The velocity of the non-charged NPs represented the velocity of the EOF and directly proportional to the electric field. No remarkable difference was observed from the migration EOF velocity values between the μCE chips with and without the bypass channel. This result indicated that the bypass channel would not produce a disturbance in the microchannel for the electrophoretic measurement. In addition, the values of EOF velocity were matched with the simulation results, expectedly. Magnitude of the EOF velocity of the experimental result (10.0 ± 0.9 μm/s for water with bypass at the applied voltage of 5 V) was coincided with the simulation result.

(a)

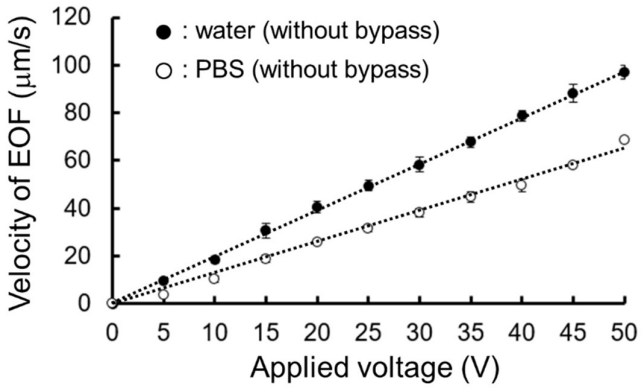

(b)

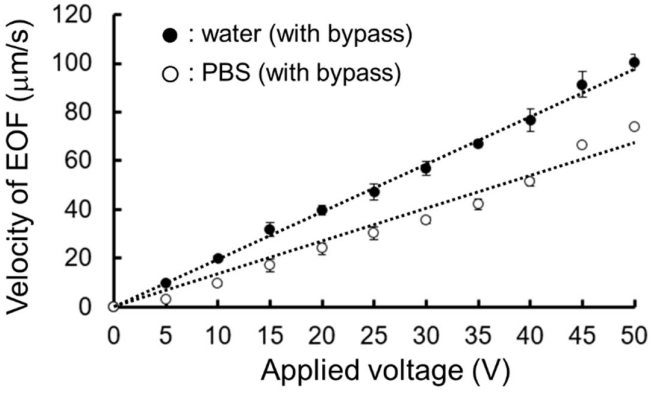

Figure 3-6 Plot of the migration velocity of the non-charged NPs (μm/s) and the applied voltage (V) for water and PBS in the μCE chip (a) without the bypass channel and (b) with the bypass channel.

3.4 Summary of this chapter

In this chapter, the experimental evaluation of the compensation of the hydrostatic pressure and Joule heating in fabricated μCE chip with the bypass channel were described. The presence of long-width bypass channel in microcapillary electrophoresis chip balance the fluid level of two open-end reservoirs and remove the hydrostatic pressure flow within the microchannel, as shown by numerical simulation, and hence, the fabricated chips were demonstrated for the evaluation of EPM by estimating the hydrostatic pressure flow compensation, current-voltage and electroosmotic flow velocity measurement in the μCE chip with and without the bypass channel.

In section 3.2.1, the fabrication steps of the microcapillary chip with and without the bypass channel were introduced. Here, soft lithography method had been employed to fabricate the μCE chips with and without the bypass channel, and made up of poly(dimethylpolysiloxane) (PDMS) and glass substrate.

In section 3.2.2, laser dark-field imaging to visualize the individual nanoparticles in the microchannel were described. In addition to the experimental setup, the principle behind this technique were also discussed. Here, the visualization and measurement of individual NPs were achieved in a dark field due to Rayleigh scattering of light in the microchannel.

In section 3.3.1, evaluation of the hydrostatic pressure compensation of the bypass channel and the stability of the fluid flow in the microchannel were described. In order to see the compensation, images of polystyrene NPs in the microchannel of the chips

were captured between 0 and 30 min, and at 1 min, 1-μL droplet of the NP suspension was added creating an imbalance in fluid level. In μCE chip without the bypass channel, low fluid conductance of the microchannel led to long balancing time. Surprisingly, we observed the fluctuation of the fluid velocity over the balancing time resulting from the meniscus instability at the fluid-wall interface called Saffman-Taylor-like meniscus instability. However, in μCE chip with the bypass channel, only Brownian motion of NPs were observed depicting the complete elimination of unstable hydrostatic pressure in the microchannel.

In section 3.3.2, the difference between the cross-sectional areas of chips and conductivities of the solutions, current-Voltage (I-V) characteristics of the μCE chip with and without the bypass channel were compared. Measured current in μCE chip with the bypass channel was 0.8–1.0 × 10^2 times higher as the large channel facilitated more ion movement. In addition, high electrical conductivity and ionic strength result in increase in the measured current for PBS. However, PBS in the μCE chip with the bypass channel resulted in a deviation from linearity over 10 V due to Joule heating accompanied with the mobility increase of the ions.

In section 3.3.3, measurement of electroosmotic flow in the chip with and without the bypass channel were discussed. In μCE chip with the bypass channel, no disturbance for the EPM measurement were observed. The magnitude of the EOF velocity of the experimental result (10.0 ± 0.9 μm/s for water in μCE chip with the bypass at the applied voltage of 5 V) was matched with the simulation result, expectedly. In addition,

EOF velocity in μCE chips with and without the bypass channel were similar depicting no disturbance in EOF due to the presence of bypass channel.

References

(55) M. Richter, P. Woias and D. Weiβ: "Microchannels for applications in liquid dosing and flow-rate measurement" Sensors and Actuators A: Physical, Vol. 62, pp. 480–483. (1997)

(56) L. Renaud, C. Malhaire, P. Kleimann, D. Barbier, P. Morin: "Theoretical and experimental studies of microflows in silicon microchannels" Materials Science and Engineering: C, Vol. 28, pp. 910–917. (2008)

(57) H. Bruus: "Theoretical microfluidics" Oxford University Press, Oxford (2008)

(58) P. G. Saffman, and G. I. Taylor: "The penetration of a fluid into a porous medium or Hele-Shaw cell containing a more viscous liquid" Proc R Soc London A, Vol. 245, pp. 312–329. (1958)

(59) S. Y. Hou, and H. Y. Chu: "Saffman-Taylor-like instability in a narrow gap induced by dielectric barrier discharge" Phys. Rev. E Stat. Nonlin. Soft Matter Phys., Vol. 92, 013101. (2015)

(60) J. H. Shiu, and H. Y. Chu: "Finger evolution of a gas bubble driven by atmospheric pressure plasma" Phys. Rev. E, Vol. 94, 063201. (2016)

CHAPTER 4

Adsorption behavior of nanoliposomes in microcapillary electrophoresis chip with the bypass channel

CHAPTER 4 Adsorption behavior of nanoliposomes in microcapillary electrophoresis chip with the bypass channel

4.1 Introduction

Chapter 4 introduce the adsorption behavior of charged nanoliposomes in presence of polymer coated on the surface of a microchannel of μCE chip with the bypass channel. The microchannel of a μCE chip is made up of poly(dimethylpolysiloxane) (PDMS), and exhibit the negative surface potential. Hence, in presence of charged nanoliposomes, there exist an electrostatic interaction between the nanoliposomes and microchannel surface.

The introduction of liposomes to the research world, more than 50 years ago[61], led to the development of numerous lipid vesicles with diverse shapes and sizes[62, 63]. A liposome is composed of an outer lipid bilayer encapsulating the internal environment. It can be uni- or multilamellar, depending on the number of bilayers, and anionic, cationic, or neutral in nature based on the charged surface. Nanoliposomes represent the lipid bilayer in nanoscale dimension, exhibiting high surface area and solubility[64, 65]. They are composed of a phospholipid and cholesterol moiety. A phospholipid is amphiphilic in nature and displays hydrophilic (phosphate ester) and hydrophobic (acyl) groups forming the bilayer, whereas the cholesterol plays a strategic role in nanoliposome composition by modulating the membrane fluidity and permeability, lipid vesicle size, and its stability[66].

A microcapillary chip which contains poly(dimethylsiloxane) (PDMS)-based sub-millimeter-sized microchannels is highly attractive for characterizing nanoparticles[38, 39]. However, the nonspecific adsorption of biomolecules and NPs onto the surface of a microchannel, owing to the interaction between the particle and microchannel surface, poses a significant challenge to this technology. These interactions can be divided into hydrophobic interaction, electrostatic with Coulombic attraction or repulsion interaction, and van der Waals interaction[67, 68]. Microcapillary chips, in many cases, are fabricated by soft lithography using PDMS and a glass substrate[30-32]. However, the surface of native PDMS in the microchannels is negatively charged. Thus, when considering a PDMS-based microcapillary chip for practical use, this negative surface potential causes:

(i) Nanoparticle adsorption due to hydrophobic and/or electrostatic interaction

(ii) Electroosmotic flow arising within the microchannel

Hence, the surface properties of a PDMS-based microchannel demand further study to determine the adsorption behavior of charged NPs in the presence of different (negative, positive, and neutral) surface zeta potentials in the microchannel. In this chapter, the adsorption phenomenon of nanoliposomes is investigated by observing the neutral, cationic, and anionic nanoliposomes in the microchannels with different surface zeta potentials. The surface zeta potential of the PDMS microchannel is changed using the neutral polyethylene-block-poly(ethylene glycol) (PEG) and a cationic

polyethylenimine (PEI) polymer coated on the microchannel.

Firstly, in section 4.2.1, the materials require to prepare the neutral, cationic and anionic nanoliposomes, and polymers to coat the PDMS microchannel are listed. In section 4.2.2, the method of preparation of nanoliposomes is described, to show the importance abd role of different molar ratio of lipids and cholesterol. In section 4.2.3, a neutral polyethylene-block-PEG and cationic PEI polymers to coat the PDMS microchannel of μCE chip and characterization of coated microchannel via non-charged nanoparticles are discussed, to give the information polymer concentration of coating. In section 4.2.4, the information about the dark-field imaging of naoliposomes in microchannel is described.

Secondly, in section 4.3.1, characterisation of nanoliposomes via measuring the avg. size, avg. zeta potential and concentration are discussed, to give the information of prepared nanoliposomes. In section 4.3.2, characterisation of coated PDMS microchannel by measuring the zeta potential of the coated microchannel using the non-charged nanoparticle is introduced, to estimate whether the PDMS microchannel is coated with the polymers or not. Finally, in section 4.3.3, adsorption dynamics of charged nanoliposomes in presence of μCE chip without coating, with cationic PEI and with the neutral polyethylene-block-PEG coating microchannel are discussed, to give the information of nanoliposomes behavior in respective coated microchannels.

4.2 Experimental procedure

4.2.1 Materials

1,2-Di-O-octadecenyl-3-trimethylammonium propane (chloride salt) (DOTMA), 1,2-dilauroyl-sn-glycero-3-phosphocholine (DLPC), and L-α-phosphatidylserine (Brain, Porcine) (sodium salt) (PS) were purchased from Avanti Polar Lipids, AL, USA, and cholesterol was purchased from Sigma Aldrich, Japan, and used without any purification. Chloroform and phosphate buffered saline (PBS) were purchased from Wako Pure Chemical Industries Ltd., Japan, and GIBCO, Invitrogen, USA, respectively. Polyethylene-block-PEG (average mol. wt. ~1400 g mol^{-1}) containing 50 wt.% ethylene oxide was purchased from Sigma Aldrich, Japan. Polyethylenimine (PEI) (average mol. wt. ~70,000 g mol^{-1}) was purchased from Fujifilm Wako Pure Chemical Corp., Japan. The noncharged NPs of polystyrene with a hydroxyl propyl cellulose coating were provided by Otsuka Electronics Co., Ltd.

4.2.2 Preparation of nanoliposomes

The nanoliposomes were prepared using the thin-film hydration method, where an appropriate molar ratio of lipids was dissolved in chloroform on a vial[69]. The lipid film was deposited by evaporating the organic solvent, and subsequently, hydrated with PBS buffer with pH 7.4 and ionic strength 165 mM for 24 h. The neutral liposome was prepared with DLPC and cholesterol at 4:1 molar ratio, which helps to maintain a similar cholesterol composition within the two monolayers of the liposome[66]. The cationic liposome was prepared with DOTMA and cholesterol at 1:1 molar ratio[71, 72], whereas the anionic liposome was prepared using DLPC, PS, and cholesterol at 5.55:0.45:4 molar ratio to avoid the saturation of the absolute value of the average zeta potential and maintaining the stability of the liposome[69]. Later, the original liposomes were extruded through a polycarbonate membrane with 100 nm pore size using an Avanti® mini-extruder to form nanoliposomes with the size distribution to study the adsorption phenomenon on the microchannel.

4.2.3 PDMS coating and characterization

A PDMS-based microchannel of a microcapillary chip with the bypass channel was coated with the following polymers: neutral polyethylene-block-PEG and cationic PEI. The PEG solution was prepared with 100 mg/mL concentration, whereas for the PEI solution, 126 mg/mL concentration was used. Later, the chip was filled with a polymer solution to coat the PDMS surface, for 4 h. In addition, to characterize the coated PDMS microchannel, 400-nm, noncharged NPs were used to estimate the zeta potential of the coated microchannel.

4.2.4 Imaging of nanoliposomes in microcapillary chips

The detection of individual nanoliposomes in the microchannel of a microcapillary chip with the bypass channel was based on dark-field imaging of the laser light scattered by the nanoliposomes exhibiting the Brownian motion under its vicinity. Here, the concentration range from 10^7 to 10^9 particles/mL are reliably detectable using the micro-capillary chip system[69]. In addition, the adsorption of nanoliposomes was estimated by image acquisition of the nanoliposome-filled microchannel with 1 min interval, starting from 4 min after liposome solution introduction in the microcapillary chip (total experiment time: 15 min). The number of nanoliposomes in the region of interest (ROI) of the microchannel was counted using the vesicle analyzer software[27] to evaluate their adsorption on the microchannel surface, as shown in Figures 4-1.

(a)

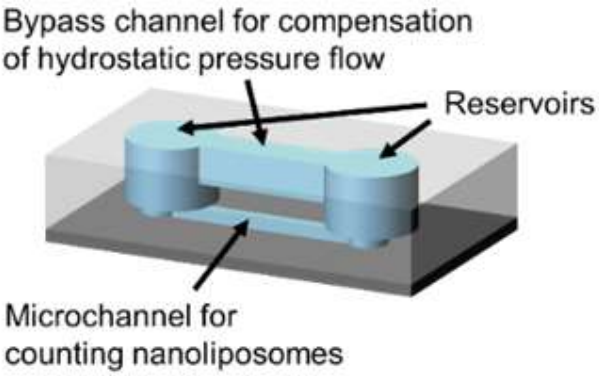

(b)

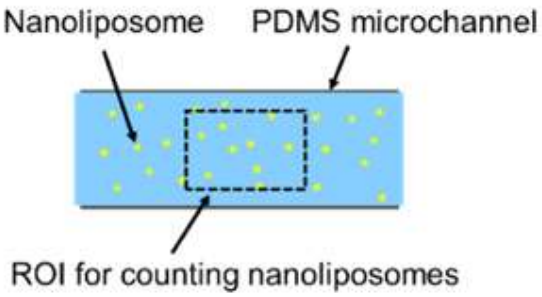

Figure 4-1 (a) Schematic of a microcapillary chip with the bypass channel. (b) Schematics of counting nanoliposomes in the PDMS microchannel of microcapillary chip with the bypass channel (200 μm width and 200 μm height).

4.3 Results and Discussion

4.3.1 Characterization of nanoliposomes

The prepared nanoliposomes were characterized for average size, polydispersity index, and zeta potential using Malvern® Zeta-Sizer Nano instrument. In addition, the nanoliposomes concentration were measured using a nanoparticle tracking analysis system (Nanosight system, Malvern) where the properties of light scattering and Brownian motion are utilize to visualize and analyze the NPs in liquid suspension based on Einstein-Stokes equation[25, 26].

4.3.1.1 Average size

Figures 4-2 show the measured average size of DLPC, DOTMA, and PS nanoliposomes, whose values were 117.0 nm, 117.3 nm, and 111.7 nm, respectively, whereas the polydispersity index (PDI) was obtained as 0.10, 0.08, and 0.08, respectively, as shown by Malvern® Zeta-Sizer Nano instrument.

(a)

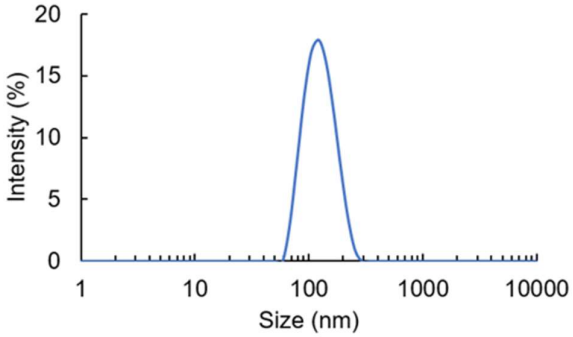

(b)

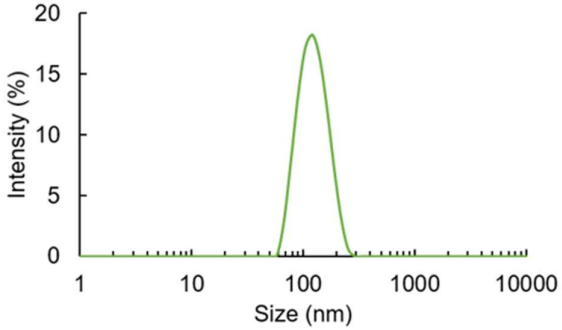

(c)

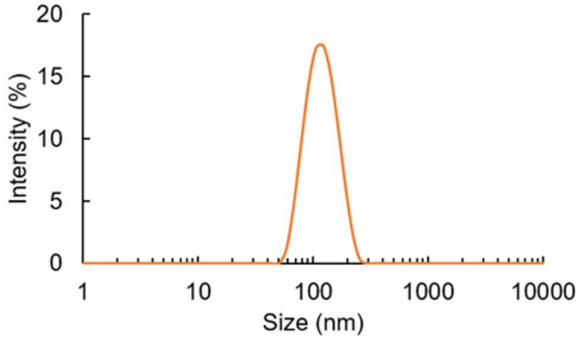

Figure 4-2 Measured average and distribution of size (nm) of nanoliposomes by Malvern® Zeta-Sizer Nano instrument: (a) DLPC, (b) DOTMA, and (c) PS.

4.3.1.2 Average zeta potential

The net charge accumulated on the liposome surface determined the magnitude and sign of zeta potential. Table 4-1 shows the average zeta potential of DLPC, DOTMA, and PS nanoliposomes. The phospholipid DLPC molecules are zwitter-ionic in nature. According to Makino et al.[72], the temperature and ionic strength of solution induces conformational changes in the lipid polar head of the liposome, and subsequently affects the zeta potential value. In the presence of a high-ionic-strength solution, the choline groups extend in the outer portion, whereas the phosphatidyl groups lie in the inner region of the liposome, resulting in a low zeta potential. Because the DLPC lipid was hydrated in PBS buffer having pH 7.4 and ionic strength 165 mM, it exhibited a low negative zeta potential. In addition, DOTMA and PS nanoliposomes showed cationic and anionic properties, respectively.

Table 4-1 Average zeta potential (mV) of DLPC, DOTMA, and PS nanoliposomes measured by Malvern® Zeta-Sizer Nano instrument.

Nanoliposomes	Average zeta potential (mV)
DLPC (neutral)	- 1.51 ± 0.19
DOTMA (cationic)	42.17 ± 1.71
PS (anionic)	-12.50 ± 0.50

4.3.1.3 Concentration of nanoliposomes

Prior to the adsorption measurement, the concentration of DLPC, DOTMA and PS nanoliposomes were measured using a nanoparticle tracking analysis system (Nanosight system, Malvern) as shown in Figures 4-3. The concentration of DLPC nanoliposomes were measured as 5.91×10^{8} particles/ml, DOTMA nanoliposomes were 34.15×10^{8} particles/ml whereas PS nanoliposomes showed 6.91×10^{8} particles/ml. Hence, 10× diluted sample of DOTMA were used in order to have an equivalent particle concentration as that of DLPC and PS nanoliposomes during the adsorption measurement in microchannel. In addition, the mean size distribution of DLPC, DOTMA and PS nanoliposomes were measured as 110 nm, 87 nm,152 nm respectively.

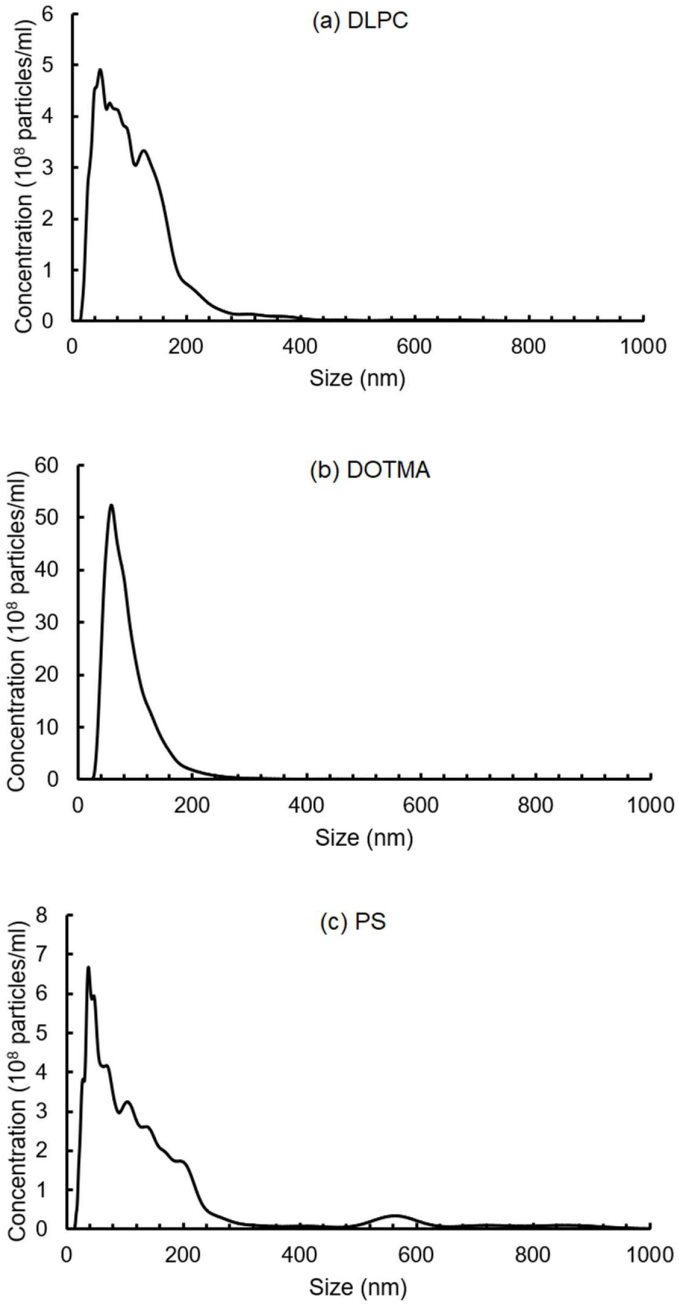

Figure 4-3 Measured concentration of nanoliposomes in nanoparticle tracking analysis (Nanosight system, Malvern) system: (a) DLPC, (b) DOTMA and (c) PS.

4.3.2 Characterization of the coated PDMS microchannel

To characterize the PDMS microchannel coated with the neutral polyethylene-block-PEG and cationic PEI, 400-nm, noncharged NPs were used as probes to estimate the surface zeta potential. Here, the velocity of the noncharged NPs represents the EOF velocity, and is directly proportional to the electric field. The zeta potential of the coated microchannel is calculated by Helmholtz–Smoluchowski equation[73]:

$$\upsilon_{EOF} = \frac{\varepsilon_0 \varepsilon E}{\eta} \zeta$$

where

υ_{EOF} : Electroosmotic flow rate in the microchannel

ζ : Zeta potential of the coated microchannel

ε : Relative permittivity of the medium

ε_0 : Vacuum permittivity

η : Viscosity of the medium

E : Electric field

The hydrophobic groups between the PDMS and polymers, namely polyethylene-block-PEG and PEI, form a weak interaction bond during the coating process, resulted in the neutral and cationic surface zeta potential in the microchannel of the microcapillary chip. Table 4-2 shows the average zeta potential of the coated microchannel.

Table 4-2 Average zeta potential (mV) of the surface of the PDMS microchannels with and without coating.

Microcapillary chip	Average zeta potential (mV)
PDMS microchannel without coating	-13.82 ± 2.31
PDMS microchannel with PEI coating	7.79 ± 0.91
PDMS microchannel with polyethylene-block-PEG coating	0.00 ± 0.01

4.3.3 Adsorption dynamics of nanoliposomes

4.3.3.1 Nanoliposomes in PDMS microchannel without coating

Figures 4-4 show the adsorption phenomena of DLPC, DOTMA, and PS nanoliposomes in the PDMS microchannel of the microcapillary chip without coating. The chemical structure of PDMS comprises repeating units of $-OSi(CH_3)_2-$ groups, leading to a hydrophobic surface within the microchannel of a microcapillary chip[74]. The particle number of neutral DLPC nanoliposomes in the ROI of the microchannel decrease gradually owing to the hydrophobic interaction with the hydrophobic surface of PDMS, and subsequently, indicate nanoliposome adsorption on the microchannel surface. In addition, the negative surface potential of PDMS results in electrostatic interaction with cationic DOTMA and anionic PS nanoliposomes arising from the Coulombic attraction or repulsion between the charged groups. Here, the decrease in the particle number of cationic DOTMA nanoliposomes represents the electrostatic attraction, whereas the fairly constant particle number of anionic PS nanoliposomes in the ROI of the microchannel show electrostatic repulsion with PDMS.

(a)

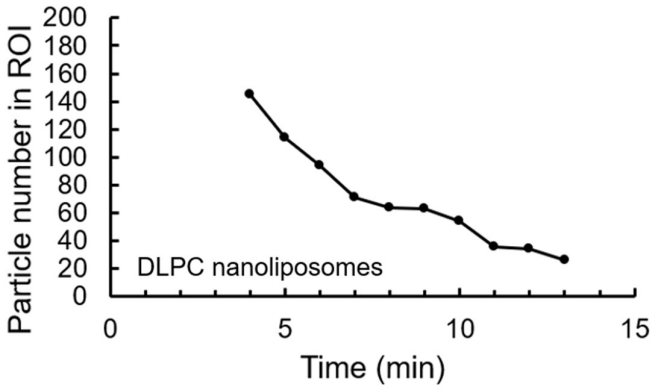

(b)

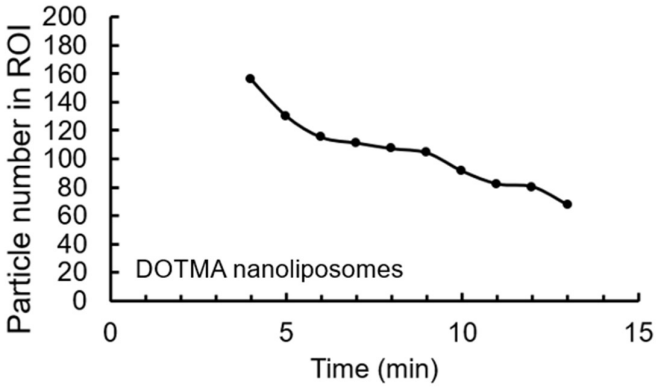

(c)

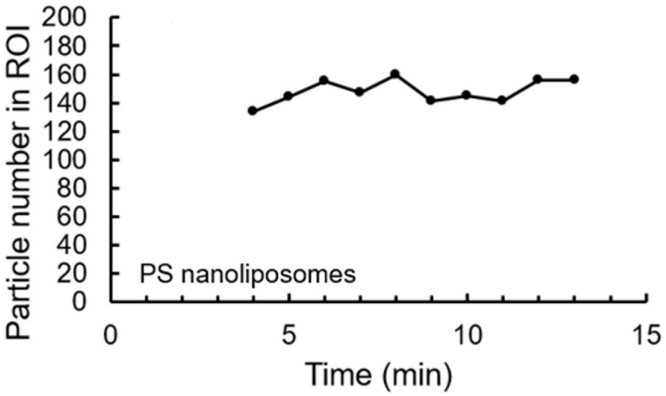

Figure 4-4 Adsorption phenomena of nanoliposomes in PDMS microchannel without coating: (a) DLPC, (b) DOTMA, and (c) PS.

4.3.3.2 Nanoliposomes in PDMS microchannel with polyethylenimine (PEI) coating

Figures 4-5 show the adsorption phenomena of DLPC, DOTMA, and PS nanoliposomes in the PDMS microchannel of the microcapillary chip with PEI coating. PEI is a polycation polymer forming a cationic coating on the PDMS surface, resulting in positive zeta potential. Owing to this, neutral DLPC nanoliposomes and cationic DOTMA nanoliposomes show the excluded volume effect and electrostatic repulsion, respectively, with the PEI-coated microchannel, as indicated by the fairly constant particle number in the ROI of the microchannel throughout the experiment. However, anionic PS nanoliposomes show a decrease in the particle number in the ROI, indicating the electrostatic interaction involving Coulombic attraction with the positively charged PEI-coated microchannel. Hence, the excluded volume effect and electrostatic repulsion of the nanoliposomes help to attenuate the adsorption in the microchannel.

(a)

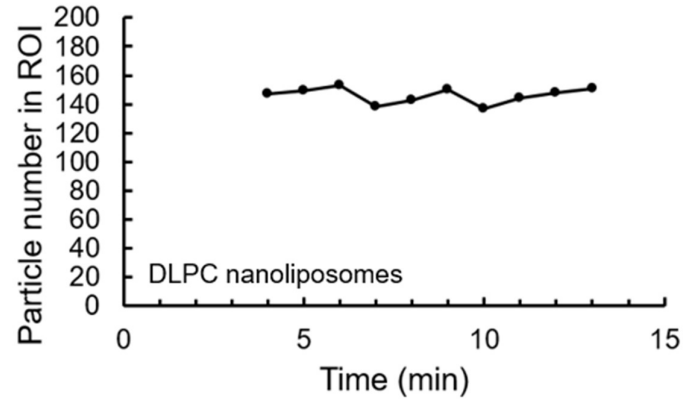

(b)

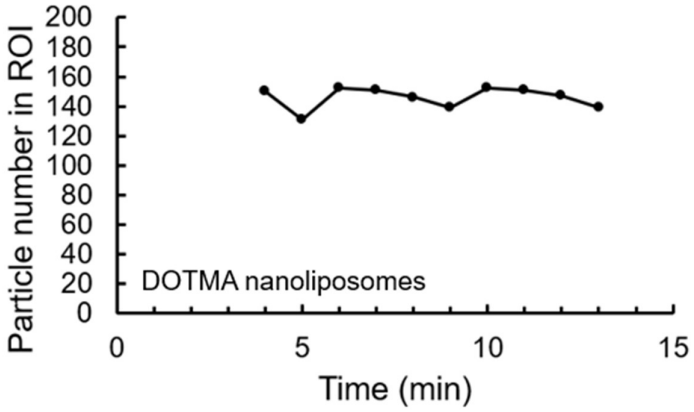

(c)

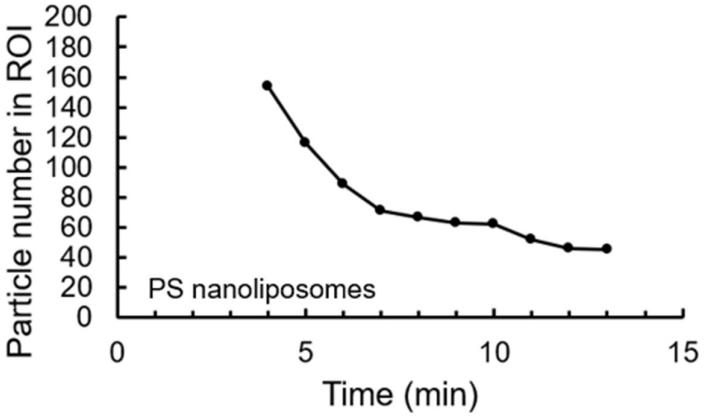

Figure 4-5 Adsorption phenomena of nanoliposomes in PDMS microchannel with PEI coating: (a) DLPC, (b) DOTMA, and (c) PS.

4.3.3.3 Nanoliposomes in PDMS microchannel with polyethylene--block-poly(ethylene glycol) (PEG) coating

Figures 4-6 show the adsorption phenomena of DLPC, DOTMA, and PS nanoliposomes in the PDMS microchannel of the microcapillary chip with the polyethylene-block-PEG coating. This coating on the PDMS leads to a neutral surface. Hence, the charged nanoliposomes display less interaction with the PEG-coated microchannel. All nanoliposomes, namely neutral DLPC, cationic DOTMA, and anionic PS, display a fairly constant particle number in the ROI, indicating the excluded volume effect with a neutral PEG-coated microchannel. Here, the PEG-derived surface modification of the microchannel leads to a significant reduction in the nonspecific interaction of nanoliposomes, causing an effective exclusion owing to the high degree of hydrophilicity and chain flexibility[75]. Therefore, the excluded volume effect of the nanoliposomes and neutral PEG-coated microchannel help to diminish the adsorption of nanoliposomes in the microchannel.

(a)

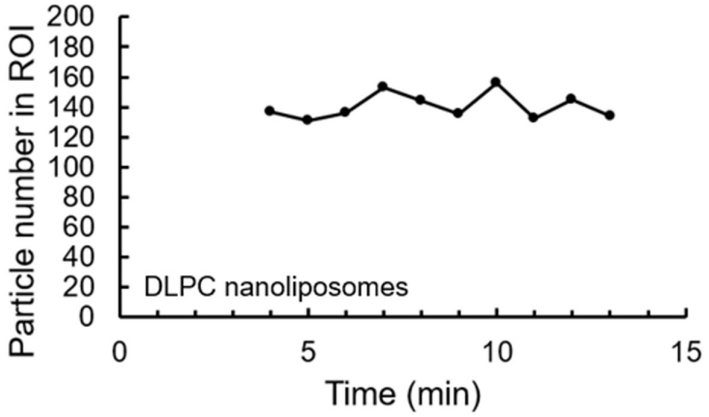

(b)

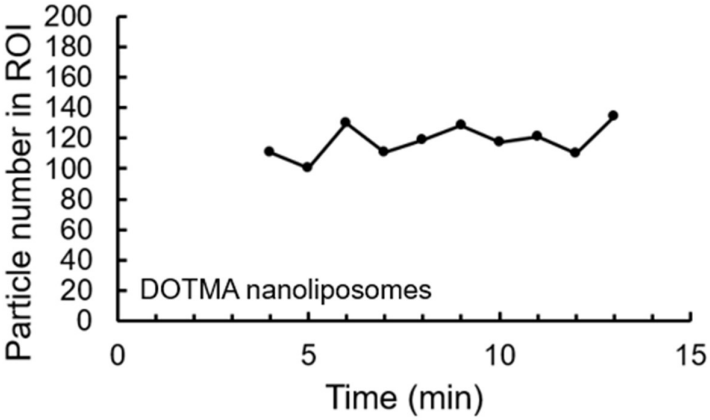

(c)

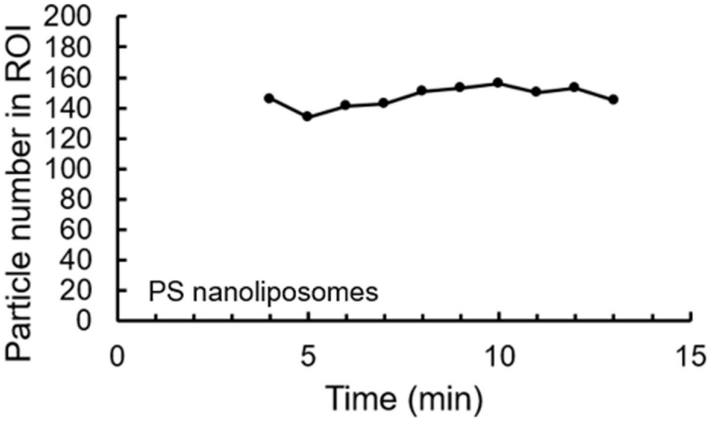

Figure 4-6 Adsorption phenomena of nanoliposomes in PDMS microchannel with polyethylene-block-PEG coating: (a) DLPC, (b) DOTMA, and (c) PS.

4.4 Summary of this chapter

In this chapter, the overview of cationic, anionic and neutral nanoliposomes exhibiting the adsorption behavior in presence of polymer (polyethylenimine and polyethylene-block-PEG) coated microchannel of a μCE chip with the bypass channel in laser dark-field were introduced. Since the PDMS-based microchannel exhibit the negative surface potential, there exist an electrostatic interaction between the nanoliposomes and surface of microchannel leading to the adsorption via hydrophobic and/or electrostatic interaction, and electroosmotic flow arising within the microchannel.

In section 4.2.1, the materials required for the preparation of neutral, cationic and anionic nanoliposomes, and polymers to coat the PDMS microchannel were introduced. Here, neutral DLPC, cationic DOTMA and anionic PS represent the charged nanoliposomes whereas polyethylenimine and polyethylene-block-PEG constitute the polymer to coat the surface of the microchannel of μCE chip.

In section 4.2.2, thin film hydration as the method of preparation of nanoliposomes was described. Here, the lipid film was deposited in vial by evaporating the organic solvent, and subsequently, hydrated with PBS buffer before the extrusion using the Avanti® mini-extruder. In addition, neutral, cationic and anionic nanoliposomes were composed of 4:1, 1:1, and 5.55:0.45:4 molar ratios, respectively, in order to maintain the effective cholesterol concentration and stability of the liposome.

In section 4.2.3, a neutral polyethylene-block-PEG and cationic PEI polymers to

coat the PDMS microchannel of μCE chip with the bypass channel was introduced. Here, 100 mg/mL and 126 mg/mL concentration of the PEG and PEI solution, respectively, for 4 h were chosen to coat the microchannel surface.

In section 4.2.4, dark-field imaging and method of image acquisition of nanoliposomes exhibitng the adsorption behavior in coated microchannel were described. With the total experiment time of 15 min, the image acquisition of the nanoliposome-filled microchannel started from 4 min, with 1 min interval, after nanoliposome solution introduction in the chip.

In section 4.3.1, avg. size, avg. zeta potential and concentration of nanoliposomes were measured as a means of characterisation. The measured average size of DLPC, DOTMA, and PS nanoliposomes were 117.0 nm, 117.3 nm, and 111.7 nm, respectively. The measured zeta potential of nanoliposomes were -1.51 ± 0.19 mV, 42.17 ± 1.71 mV, and -12.50 ± 0.50 mV, respectively. In addition, 5.91×10^8 particles/ml, 34.15×10^8 particles/ml, and 6.91×10^8 particles/ml represent the concentration of neutral DLPC, cationic DOTMA and anionic PS nanoliposomes measured by NTA system.

In section 4.3.2, zeta potential of the coated microchannel using the 400-nm non-charged nanoparticles were employed to characterise the polymer-coated PDMS microchannel. Here, the calculated zeta potential of PDMS microchannel without coating, with PEI coating and with polyethylene-block-PEG were -13.82 ± 2.31 mV, 7.79 ± 0.91 mV, and 0.00 ± 0.01 mV, respectively.

In section 4.3.3, adsorption behavior of neutral DLPC, cationic DOTMA and

anionic PS nanoliposomes in PDMS microchannel without coating, with cationic PEI and with neutral polyethylene-block-PEG coating were discussed. Firstly, in subsection 4.3.3.1, in PDMS microchannel without coating, the decrease in the particle number of neutral DLPC and cationic DOTMA nanoliposomes suggested the hydrophobic interaction with the hydrophobic surface and electrostatic interaction with the negative surface potential of PDMS, respectively. However, anionic PS nanoliposomes showed the electrostatic repulsion with PDMS. Secondly, in subsection 4.3.3.2, in PDMS microchannel with cationic PEI coating, the fairly constant particle number of neutral DLPC and cationic DOTMA nanoliposomes showed the excluded volume effect and electrostatic repulsion, respectively whereas PS nanoliposomes exhibit the electrostatic attraction. Finally, in subsection 4.3.3.3, in PDMS microchannel with polyethylene-block-PEG coating, all the nanoliposomes displayed the excluded volume effect as indicated by the constant particle number in the ROI. Therefore, we concluded that the electrostatic repulsion and excluded volume effect helps to attenuate the adsorption of nanoliposomes on the PDMS-based microchannel surface.

References

(61) A. D. Bangham, M. M. Standish, and J. C. Watkins: “Diffusion of univalent ions across the lamellae of swollen phospholipids" J. Mol. Biol., Vol. 13, pp. 238–252. (1965)

(62) M. R. Mozafari, and S. M. Mortazavi (eds): “Nanoliposomes: from fundamentals to recent developments” Trafford Publishing Co. Ltd, Oxford, UK (2005)

(63) M. R. Mozafari: “Nanoliposomes: preparation and analysis.” In: Weissig V. (eds) Liposomes. Methods in Molecular Biology (Methods and Protocols), 605, Humana Press (2010)

(64) M. R. Mozafari (ed): “Nanocarrier technologies: frontiers of nanotherapy” Springer, The Netherlands (2006)

(65) G. X. Zhai, G. G. Chen, Y. Zhao, H. X. Lou, and J. S. Zhang: "Study on preparation of low molecular weight heparin nanoliposomes and their oral absorption in rat" J. China Pharm. Univ., Vol. 33, pp. 200–202. (2002)

(66) F. Szoka, and D. Papahadjopoulos: "Comparative Properties and Methods of Preparation of Lipid Vesicles (Liposomes)" Ann. Rev. Biophys. Bioeng., Vol. 9, pp. 467–508. (1980)

(67) J. Y. Yoon, and R. L. Garrell: “Biomolecular adsorption in microfluidics.” In: Li D. (eds) Encyclopedia of Microfluidics and Nanofluidics. Springer, Boston, MA (2008)

(68) K. Y. Chumbimuni-Torres, R. E. Coronado, A. M. Mfuh, C. Castro-Guerrero, M. F. Silva, G. R. Negrete, R. Bizios, and C. D. Garcia1: "Adsorption of Proteins to Thin-Films of PDMS and Its Effect on the Adhesion of Human Endothelial Cells" Royal Society of Chemistry Advances, Vol. 1, pp. 706–714. (2011)

(69) K. Kato, M. Koido, M. Kobayashi, T. Akagi, and T. Ichiki: "Statistical fluctuation in zeta potential distribution of nanoliposomes measured by on-chip microcapillary electrophoresis" Electrophoresis, Vol. 34, pp. 1212–1218. (2013)

(70) S. Kawakami, A. Harada, K. Sakanaka, K. Nishida, J. Nakamura, T. Sakaeda, N. Ichikawa, M. Nakashima, and H. Sasaki: "In vivo gene transfection via intravitreal injection of cationic liposome/plasmid DNA complexes in rabbits" International Journal of Pharmaceutics, Vol. 278, pp. 255–262. (2004)

(71) Y. Hattori, S. Arai, T. Kikuchi, M. Hamada, R. Okamoto, Y. Machida, and K. Kawano: "Optimization of siRNA Delivery Method into the Liver by Sequential

Injection of Polyglutamic Acid and Cationic Lipoplex" Pharmacology & Pharmacy, Vol. 6, pp. 302–310. (2015)

(72) K. Makino, T. Yamada, M. Kimura, T. Oka, H. Ohshima, and T. Kondo: "Temperature- and ionic strength-induced conformational changes in the lipid head group region of liposomes as suggested by zeta potential data" Biophysical Chemistry, Vol. 41, pp. 175–183. (1991)

(73) A. Inagawa, M. Fukuyama, A. Hibara, M. Harada, and T. Okada: "Zeta potential determination with a microchannel fabricated in solidified solvents" Journal of Colloid and Interface Science, Vol. 532, pp. 231–235. (2018)

(74) J. N. Lee, C. Park, and G. M. Whitesides: "Solvent Compatibility of Poly(dimethylsiloxane)-Based Microfluidic Devices" Anal. Chem., Vol. 75, pp. 6544–6554. (2003)

(75) J. M. Harris (ed): “Poly(ethylene glycol) chemistry, biotechnical and biomedical applications” Plenum Press, New York (1992)

CHAPTER 5

Temperature dependent adsorption behavior of nanoliposomes on PEG-modified surface

CHAPTER 5 Temperature dependent adsorption behavior of nanoliposomes on PEG-modified surface

5.1 Introduction

In the previous chapter, the adsorption behavior of charged nanoliposomes in presence of polymer coated on the surface of a microchannel of μCE chip with the bypass channel were studied as part of the fundamental of this thesis. Brownian motion of nanoliposomes were stably observed and adsorption of nanoliposomes on the surface of the microchannel can be attenuated based on electrostatic repulsion and excluded volume effect. Chapter 5 deal with the application of the μCE chip with the bypass channel. In this study, the effect of temperature on adsorption behavior of nanoliposomes on polyethylene-block-PEG coated PDMS microchannel of μCE chip with the bypass channel are observed.

PEG is a non-toxic, hygroscopic, and chemically inert synthetic polymer with the application ranging from the PEG-grafted liposomes[76] to polymer coating[77]. The properties of PEG can be affected by its molecular weight, temperature and even the presence of additives[78]. However, there are not much reported studies on the effect of temperature on PEG-modified surface for adsorption behavior of nanoliposomes. Hence, in this study, temperature dependent adsorption behavior of 50-nm, 100-nm, and 150-nm DLPC nanoliposomes on polyethylene-block-PEG coated PDMS microchannel of μCE chip with the bypass channel are investigated.

Firstly, in section 5.2, preparation of 50-nm, 100-nm, and 150-nm DLPC nanoliposomes, PDMS-based microchannel coated with the neutral polyethylene-block-PEG polymer, and dark-field imaging in the microchannel are briefly discussed. Secondly, in section 5.3.1, characterisation of DLPC nanoliposomes via measuring the avg. size, avg. zeta potential and concentration are discussed, to give the information of prepared nanoliposomes. Thirdly, in section 5.3.2, DLPC nanoliposomes in PEG-coated PDMS microchannel at room temperature is observed. Finally, in section 5.3.3, DLPC nanoliposomes in PEG-coated PDMS microchannel at gradual increase in temperature is discussed.

5.2 Experimental procedure

5.2.1 Materials

1,2-dilauroyl-sn-glycero-3-phosphocholine (DLPC), and cholesterol were purchased from Avanti Polar Lipids, AL, USA, and Sigma Aldrich, Japan, respectively, and used without any purification. Chloroform and phosphate buffered saline (PBS) were purchased from Wako Pure Chemical Industries Ltd., Japan, and GIBCO, Invitrogen, USA, respectively. Polyethylene-block-PEG (average mol. wt. ~1400 g mol^{-1}) containing 50 wt.% ethylene oxide was purchased from Sigma Aldrich, Japan.

5.2.2 Preparation of DLPC nanoliposomes

As described in chapter 4, the liposomes were prepared using the thin-film hydration method, where DLPC and cholesterol at 4:1 molar ratio was dissolved in chloroform on a vial. The lipid film was deposited by evaporating the organic solvent, and subsequently, hydrated with PBS buffer with pH 7.4 and ionic strength 165 mM for 24 h. Later, the original liposomes were extruded through a polycarbonate membrane with 50-nm, 100-nm and 150-nm pore size using an Avanti® mini-extruder to form nanoliposomes with the appropriate size distribution.

5.2.3 PDMS coating with neutral polyethylene-block-PEG polymer

A PDMS-based microchannel of a microcapillary chip with the bypass channel was coated with 100 mg/mL concentration of neutral polyethylene-block-PEG polymer for 4 h as described in chapter 4.

5.2.4 Imaging of DLPC nanoliposomes in microcapillary chips

As described in chapter 4, the detection of individual DLPC nanoliposomes in the microchannel of a μCE chip with the bypass channel was based on dark-field imaging. To study the temperature dependent adsorption behavior of nanoliposomes on PEG-modified surface, the image acquisition of the nanoliposomes at room and gradual increase in temperature in microchannel were taken, with 1 min interval, starting from 4 min after solution introduction in the microcapillary chip (total experiment time: 15 min). Later the number of nanoliposomes in the region of interest (ROI) of the microchannel was counted using the vesicle analyzer software.

5.3 Results and Discussion

5.3.1 Characterization of DLPC nanoliposomes

The prepared 50-nm, 100-nm, and 150-nm DLPC nanoliposomes were characterized for average size, polydispersity index, and zeta potential using Malvern® Zeta-Sizer Nano instrument. In addition, the liposomes concentration was measured using a nanoparticle tracking analysis system (Nanosight system, Malvern) as described in chapter 4.

5.3.1.1 Average size

Figures 5-1 show the measured average size of DLPC nanoliposomes, whose values were 69.42 nm, 108.9 nm, and 154.5 nm, respectively, whereas the polydispersity index was obtained as 0.073, 0.065, and 0.109, respectively, as shown by Malvern® Zeta-Sizer Nano instrument.

(a)

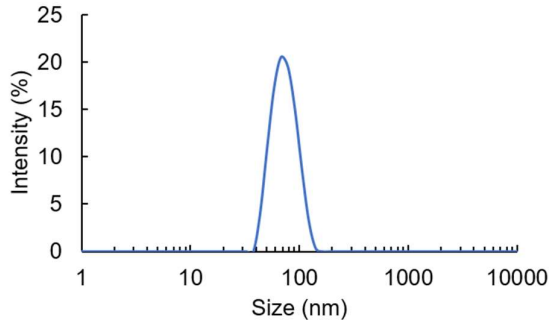

(b)

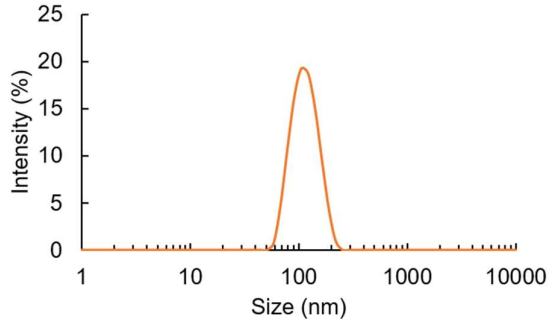

(c)

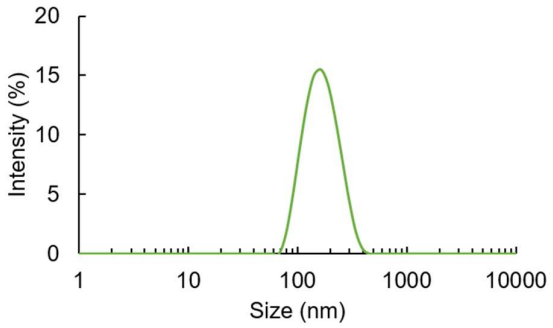

Figure 5-1 Measured average and distribution of size (nm) of DLPC nanoliposomes by Malvern® Zeta-Sizer Nano instrument: (a) 50 nm, (b) 100 nm, and (c) 150 nm.

5.3.1.2 Average zeta potential

The net charge accumulated on the liposome surface determined the magnitude and sign of zeta potential. Table 5-1 shows the average zeta potential of 50-nm, 100-nm, and 150-nm DLPC nanoliposomes measured by Malvern® Zeta-Sizer Nano instrument.

Table 5-1 Average zeta potential (mV) of 50-nm, 100-nm, and 150-nm DLPC nanoliposomes measured by Malvern® Zeta-Sizer Nano instrument.

Liposomes	Average zeta potential (mV)
50-nm DLPC	-1.28 ± 0.62
100-nm DLPC	-1.07 ± 0.34
150-nm DLPC	-0.94 ± 0.30

5.3.1.3 Concentration of DLPC nanoliposomes

Prior to the temperature dependent adsorption behavior in μCE with the bypass channel, the concentration of 50-nm, 100-nm, and 150-nm DLPC nanoliposomes were measured using a nanoparticle tracking analysis system (Nanosight system, Malvern) as shown in Figures 5-2. The concentration of 50-nm DLPC nanoliposomes were measured as 46.30×10^8 particles/ml, 100-nm DLPC nanoliposomes were 10.07×10^8 particles/ml whereas 150-nm DLPC nanoliposomes showed 26.69×10^8 particles/ml. In addition, the mean size distribution of 50-nm, 100-nm, and 150-nm DLPC nanoliposomes were measured as 50 nm, 143 nm, and 182 nm respectively. Later, an average particle concentration of 1×10^8 particles/mL for each DLPC nanoliposomes were prepared to study the adsorption behavior on PEG-modified PDMS microchannel of μCE with the bypass channel at different temperature.

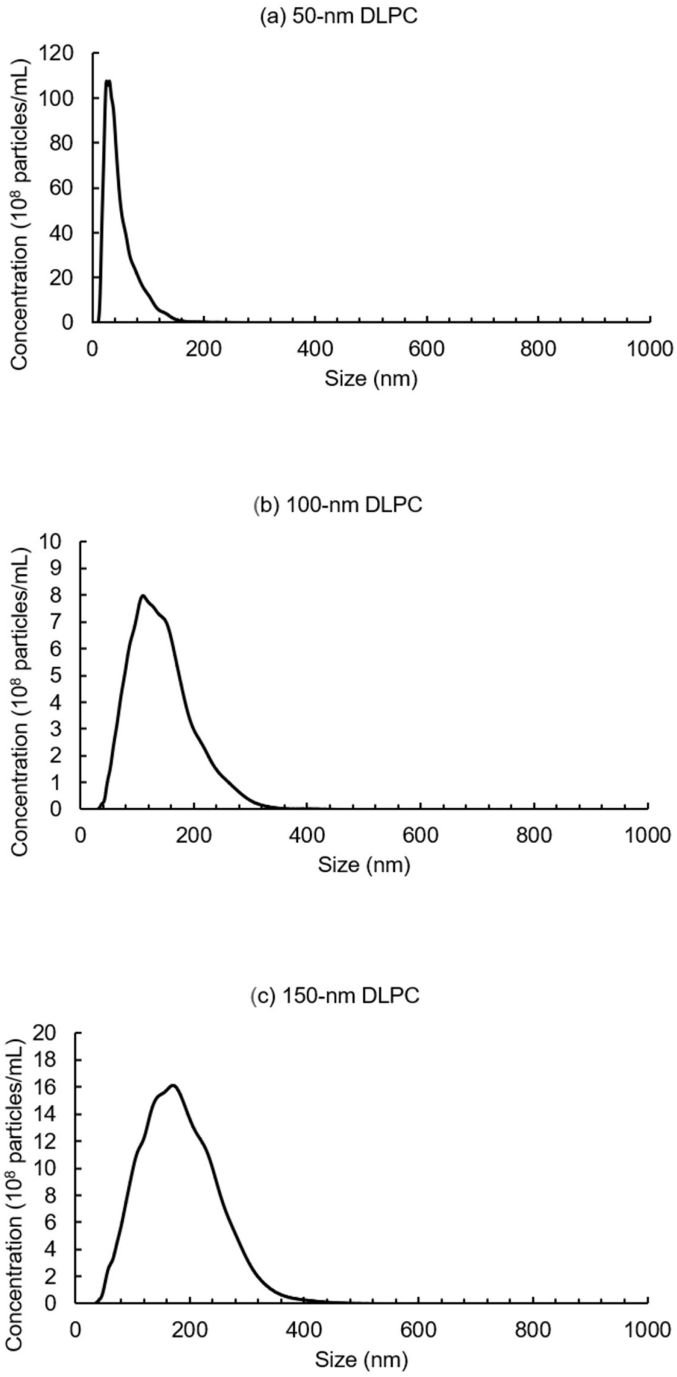

Figure 5-2 Measured concentration of DLPC nanoliposomes in nanoparticle tracking analysis system (Nanosight system, Malvern): (a) 50-nm, (b) 100-nm, and (c) 150-nm.

5.3.2 DLPC nanoliposomes in PEG-coated PDMS microchannel at room temperature

Figures 5-3 show the zeta potential of 50-nm, 100-nm, and 150-nm DLPC nanoliposomes in the polyethylene-block-PEG coated PDMS microchannel of the microcapillary chip with the bypass channel at room temperature. Here, DLPC nanoliposomes show the average low zeta potential owing to the high ionic strength of PBS solution as described in chapter 4. Figures 5-4 show the particle number in ROI for 50-nm, 100-nm, and 150-nm DLPC nanoliposomes in the polyethylene-block-PEG coated PDMS microchannel of the microcapillary chip with the bypass channel at room temperature. PEG-coating on the PDMS microchannel led to a neutral surface, and hence, DLPC nanoliposomes display excluded volume effect as indicated by fairly constant particle number in the ROI throughout the experiment.

(a)

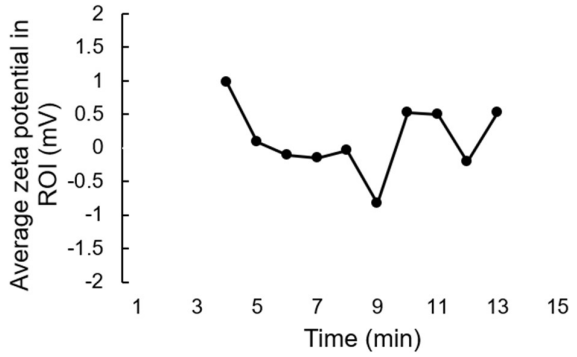

(b)

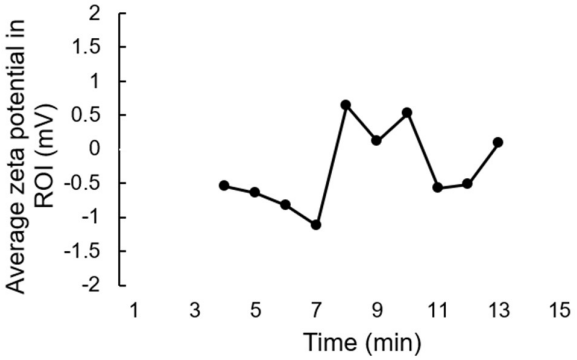

(c)

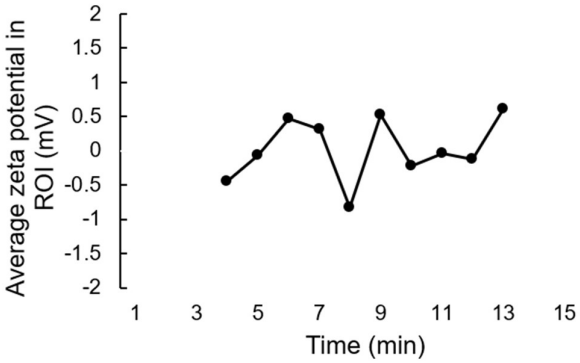

Figure 5-3 Zeta potential of DLPC nanoliposomes in polyethylene-block-PEG coated PDMS microchannel of a μCE chip with the bypass channel at room temperature measured by vesicle analyzer software: (a) 50-nm, (b) 100-nm, and (c) 150-nm.

(a)

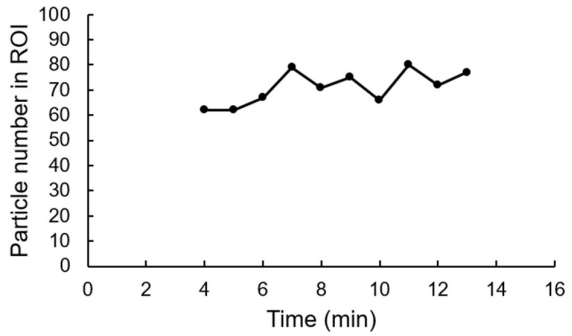

(b)

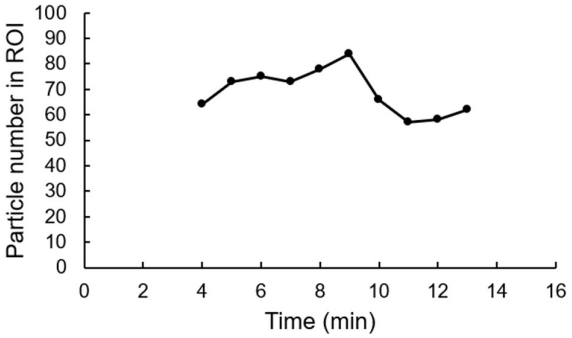

(c)

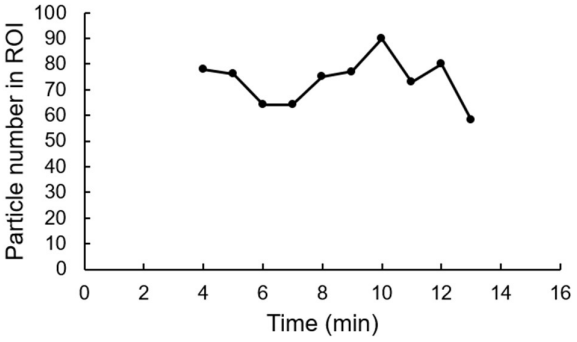

Figure 5-4 Particle number of DLPC nanoliposomes in ROI in polyethylene-block-PEG coated PDMS microchannel of a μCE chip with the bypass channel at room temperature measured by vesicle analyzer software: (a) 50-nm, (b) 100-nm, and (c) 150-nm.

5.3.3 DLPC nanoliposomes in PEG-coated PDMS microchannel at gradual increase in temperature

Figures 5-5 show the zeta potential of 50-nm, 100-nm, and 150-nm DLPC nanoliposomes in the polyethylene-block-PEG coated PDMS microchannel of the microcapillary chip with the bypass channel at gradual increase in temperature. Here, initially DLPC nanoliposomes were kept at low temperature (3-4 °C) whereas PEG-coated μCE chip with the bypass channel and vesicle analyzer at room temperature. Hence, image acquisition of adsorption behavior of nanoliposomes were obtained in gradual increase in temperature condition. Figures 5-6 show the particle number in ROI for 50-nm, 100-nm, and 150-nm DLPC nanoliposomes in the polyethylene-block-PEG coated PDMS microchannel of a μCE chip with the bypass channel at gradual increase in temperature. As observed earlier, PEG-coated microchannel exhibit the excluded volume effect with the nanoliposomes at room temperature, however, we observed a gradual increase in the particle number in ROI for all the nanoliposomes signifying the high adsorption coefficient and inefficiency of excluded volume effect for PEG at low temperature.

(a)

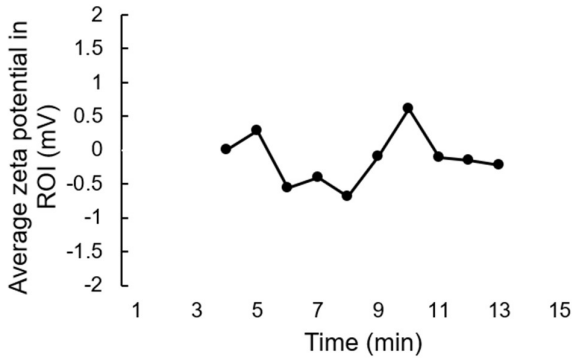

(b)

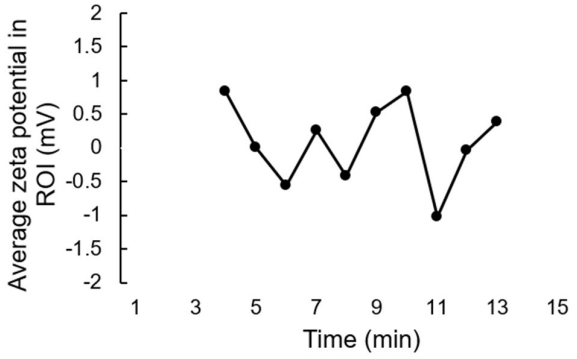

(c)

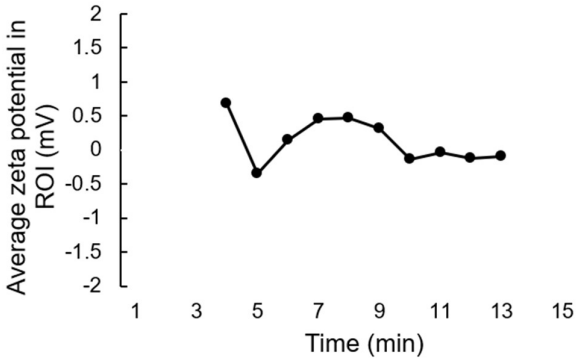

Figure 5-5 Zeta potential of DLPC nanoliposomes in polyethylene-block-PEG coated PDMS microchannel of a μCE chip with the bypass channel at gradual increase in temperature measured by vesicle analyzer software: (a) 50-nm, (b) 100-nm, and (c) 150-nm.

(a)

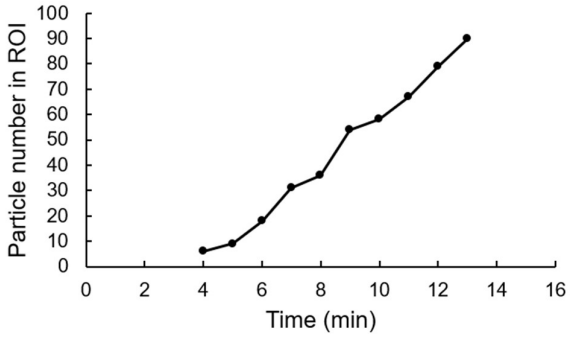

(b)

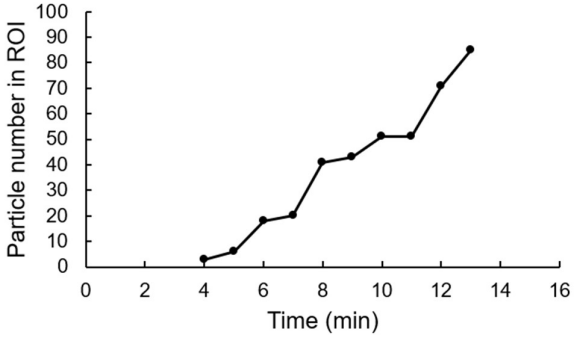

(c)

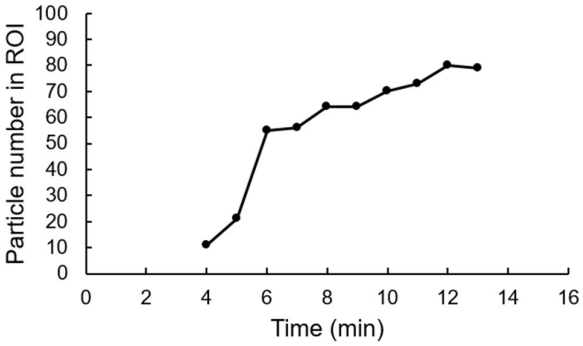

Figure 5-6 Particle number in ROI for DLPC nanoliposomes in polyethylene-block-PEG coated PDMS microchannel of a μCE chip with the bypass channel at gradual increase in temperature measured by vesicle analyzer software: (a) 50-nm, (b) 100-nm, and (c) 150-nm.

5.4 Summary of this chapter

In this chapter, the overview of the effect of temperature on adsorption behavior of nanoliposomes on polyethylene-block-PEG coated PDMS microchannel of μCE chip with the bypass channel were introduced. DLPC nanoliposomes-filled chips were kept at room and gradual increase in temperature condition, and their adsorption behavior were observed using the laser dark-field imaging.

In section 5.2.1, the materials required for the preparation of 50-nm, 100-nm, and 150-nm neutral DLPC nanoliposomes, polymers to coat the PDMS microchannel of μCE chip with the bypass channel were introduced.

In section 5.2.2, thin film hydration as the method of preparation of nanoliposomes was described. Here, the lipid film with 4:1 molar ratio was deposited in vial by evaporating the organic solvent, and subsequently, hydrated with PBS buffer before the extrusion using the Avanti® mini-extruder to form 50-nm, 100-nm, and 150-nm DLPC nanoliposomes.

In section 5.2.3, a neutral polyethylene-block-PEG polymer to coat the PDMS microchannel of μCE chip with the bypass channel was introduced. Here, 100 mg/mL concentration of the PEG solution for 4 h was chosen to coat the microchannel surface as described in chapter 4.

In section 5.2.4, dark-field imaging and method of image acquisition of nanoliposomes exhibitng the adsorption phenomena in coated microchannel were described. With the total experiment time of 15 min, the image acquisition of the

nanoliposomes-filled microchannel started from 4 min, with 1 min interval, after solution introduction in the chip.

In section 5.3.1, avg. size, avg. zeta potential and concentration of nanoliposomes were measured as a means of characterisation. The measured average size of 50-nm, 100-nm, and 150-nm DLPC liposomes were 69.42 nm, 108.9 nm, and 154.5 nm, respectively. The measured zeta potential were -1.28 ± 0.62 mV, -1.07 ± 0.34 mV, and -0.94 ± 0.30 mV, respectively. In addition, 46.30×10^8 particles/ml, 10.07×10^8 particles/ml, and 26.69×10^8 particles/ml represent the concentration of 50-nm, 100-nm, and 150-nm DLPC nanoliposomes measured by NTA system.

In section 5.3.2, zeta potential and particle number in ROI of 50-nm, 100-nm, and 150-nm DLPC nanoliposomes in polyethylene-block-PEG coated PDMS microchannel of a μCE chip with the bypass channel at room temperature were introduced. All the nanoliposomes showed the average low zeta potential owing to the high ionic strength of PBS solution and displayed a fairly constant particle number in the ROI throughout the experiment.

In section 5.3.3, zeta potential and particle number in ROI of 50-nm, 100-nm, and 150-nm DLPC nanoliposomes in polyethylene-block-PEG coated PDMS microchannel of a μCE chip with the bypass channel at gradual increase in temperature were introduced. Here, initially DLPC nanoliposomes were kept at low temperature (3-4 °C) whereas PEG-coated μCE chip with the bypass channel and vesicle analyzer at room temperature. We observed a gradual increase in the particle number in ROI for all the

nanoliposomes suggesting the high adsorption coefficient and inefficiency of excluded volume effect for PEG at low temperature.

References

(76) O. Tirosh, Y. Barenholz, J. Katzhendler, and A. Priev: "Hydration of Polyethylene Glycol-Grafted Liposomes" Biophysical Journal, Vol. 74, pp. 1371–1379. (1998)

(77) M. Malmsten, K. Emoto, and J. M. Van Alstine: "Effect of Chain Density on Inhibition of Protein Adsorption by Poly(ethylene glycol) Based Coatings" Journal of Colloid and Interface Science, Vol. 202, pp. 507–517. (1998)

(78) J. A. Baird, R. Olayo-Valles, C. Rinaldi, and L. S. Taylor: "Effect of molecular weight, temperature, and additives on the moisture sorption properties of polyethylene glycol" J Pharm Sci., Vol. 99, pp. 154–168. (2010)

CHAPTER 6

General summary

CHAPTER 6 General Summary

The present work is the study to develop an analysis platform for nanoparticles by extending the potential applicability of the microcapillary electrophoresis chip. This work facilitates the technological advancement in μCE chip with new design by adding long-width bypass channel to balance the fluid level of two open-end reservoirs to compensate the hydrostatic pressure flow in a microchannel, and thereby, enhancing the accurate measurement of electrophoretic mobility and zeta potential of individual nanoparticle.

Chapter 1 provided the general introduction about the nanoparticles and the numerous characterization techniques with on-going R&D and future prospect. A new characterization method using the microcapillary electrophoresis chip for extracellular vesicles including the exosomes has been discussed. In addition, the detail overview of the issues in the microcapillary electrophoresis chip, namely, hydrodynamic issue arising due to the low fluid conductance of the microchannel, electrochemical or Joule heating issue due to increase in the ion mobility, and adsorption issue due to negative surface potential of PDMS-based microchannel; hindering the accurate measurement of EPM of nanoparticle with the proposed research targets to solve the issues in the chip were discussed. Finally, aim of this study, flow and structure of this thesis proposes to develop an analytical method for nanoparticle characterization by incorporating the

unresolved issues.

Chapter 2 provided the overview of simulation of fluid level adjustment for air-water interface with laminar and phase field in μCE chip with the long-width bypass channel. To simulate the two-phase interface, the appropriate model materials, parameters, and boundary conditions were applied. The model equations such as Navier-Stokes equation for the flow in the channel, electroosmotic velocity and the electric field strength governing by Helmholtz-Smoluchowski, air-water interface motion by Cahn-Hilliard equation and phase field, and contact angle by wetted wall were coupled. Finally, the simulated results of the μCE chip with the bypass channel showed the volume fraction of fluid and fluid velocity distribution at the applied electric potential of 5 V depicting the presence of hydrostatic counter flow in the bypass channel to compensate the unbalanced hydrostatic pressure. Hence, the above results provided the assumption that addition of long-width bypass channel helps to compensate the hydrostatic pressure flow in the microchannel.

Chapter 3 provided the experimental evaluation of the compensation of the hydrostatic pressure and Joule heating in μCE chip with the bypass channel and the obtained results were compared with that of the simulated. Firstly, μCE chip with and without the bypass channel were fabricated and individual NPs measurement were achieved by laser dark-field imaging in the microchannel. To verify the compensation of

the hydrostatic pressure in chips, images of polystyrene NPs in the microchannel were captured between 0 and 30 min, and at 1 min, 1-μL droplet of the NP suspension was added. Surprisingly, in μCE chip without the bypass channel, we observed the fluctuation of the fluid velocity over the balancing time resulting from the meniscus instability at the fluid-wall interface called Saffman-Taylor-like meniscus instability. However, in μCE chip with the bypass channel, only Brownian motion of NPs were observed depicting the complete elimination of unstable hydrostatic pressure in the microchannel. Secondly, current-Voltage (I-V) characteristics of the μCE chips with and without the bypass channel were compared since the chips have the different cross-sectional areas and use of solution with different conductivity. The obtained results for measured current was 0.8–1.0 × 10^2 times higher in μCE chip with the bypass channel. In addition, high electrical conductivity and ionic strength result in increase in the measured current for phosphate buffered saline (PBS) with deviation from linearity was observed over 10 V due to Joule heating. Lastly, EOF velocity of non-charged NPs from the experimental result was matched with the simulated result and showed no remarkable difference in EOF value in chips. Hence, the above result provided the conclusion that addition of bypass channel has no effect on EOF value.

Chapter 4 provided the information about the adsorption behavior of neutral 1,2-dilauroyl-sn-glycero-3-phosphocholine (DLPC), cationic 1,2-Di-O-octadecenyl-3-trimethylammonium propane (DOTMA), and anionic

L-α-phosphatidylserine (PS) nanoliposomes in presence of cationic polyethylenimine (PEI) and neutral polyethylene-block-PEG polymer-coated PDMS microchannel of μCE chip with the bypass channel. DLPC, DOTMA, and PS nanoliposomes were prepared by thin film hydration method with 4:1, 1:1, and 5.55:0.45:4 molar ratios, respectively, and extruded to 100 nm size. The polymer-coated PDMS microchannel were characterized by non-charged nanoparticles. Firstly, the observed results for PDMS microchannel without coating showed the hydrophobic and electrostatic interaction for DLPC and DOTMA nanoliposomes, respectively, whereas PS nanoliposome showed the electrostatic repulsion. Secondly, PDMS microchannel with PEI coating, DLPC and DOTMA nanoliposomes showed the excluded volume effect and electrostatic repulsion, respectively, whereas PS nanoliposome exhibited the electrostatic attraction. Finally, with polyethylene-block-PEG coated PDMS microchannel, all the nanoliposomes showed the excluded volume effect. Therefore, the above results provided the conclusion that adsorption phenomena of the nanoliposomes on the microchannel surface arose from hydrophobic and electrostatic interaction, and can be attenuated based on electrostatic repulsion and the excluded volume effect.

Chapter 5 provided the overview of temperature dependent adsorption behavior of 50-nm, 100-nm, and 150-nm DLPC nanoliposomes on polyethylene-block-PEG coated microchannel of μCE chip with the bypass channel in laser dark-field. The prepared DLPC nanoliposomes were characterized for avg. size, avg. zeta potential, and

concentration; and subjected to adsorption measurement at room and gradual increase in temperature respectively. Firstly, nanoliposomes in chip at room temperature showed the excluded volume effect with fairly constant particle number in ROI and low zeta potential owing to the high ionic strength of PBS solution as expected. Later, adsorption behavior of nanoliposomes in chip at gradual increase in temperature were observed, and surprisingly, nanoliposomes showed the gradual increase in the particle number in ROI due to high adsorption coefficient and inefficiency of excluded volume effect of PEG at low temperature. Therefore, the above observed results provided the information about the temperature dependent adsorption behavior of nanoliposomes on PEG-coated surface.

We have successfully developed an analysis platform for nanoparticles by extending the potential applicability of the microcapillary electrophoresis chip with new design and improved the accuracy in electrophoretic measurement. This analytical platform can augment the use and application of a microcapillary chip in the field of materials engineering. The importance of this chip can be recognized as a fundamental tool especially for the characterization of extracellular vesicles (EVs) including exosomes, and application in the field of nanobiotechnology.

The future perspective of nanoparticle characterization depends on the development of an analytical platform providing the range of nanoparticle properties within the single

device. These properties, in general, can be divided into the multiparametric profiling of nanoparticle, target surface marker and dynamic state profiling between the nanoparticle and the biological membrane, etc. In addition, the future perspective with the application of the microcapillary electrophoresis chip with the bypass channel is to study the zeta potential and surface charge of nanoliposomes in presence of hydrolytic enzyme in laser dark-field imaging. Since the zeta potential of nanoliposomes are irrespective of their size and concentration, it would be an interesting study to investigate whether the similar concentration of nanoliposomes demonstrate the similar change in zeta potential in presence of same concentration of hydrolytic enzyme in μCE chip with the bypass channel.

Acknowledgements

First and foremost, the author wishes to express his sincere gratitude to Professor Dr. Takanori Ichiki at Department of Materials Engineering, Graduate School of Engineering, the University of Tokyo for his supervision, generous assistance, acuity and encouragements for the completion of this thesis.

The author wishes to express sincere gratitude to Assistant Professor Dr. Hiroaki Takehara at Department of Materials Engineering, Graduate School of Engineering, the University of Tokyo for valuable discussion and suggestion.

The author would like to express sincere respect to Professor Dr. Madoka Takai at Department of Bioengineering, Graduate School of Engineering, the University of Tokyo, Associate Professor Dr. Hirotaka Ejima at Department of Materials Engineering, Graduate School of Engineering, the University of Tokyo, Associate Professor Dr. Kanjiro Miyata at Department of Materials Engineering, Graduate School of Engineering, the University of Tokyo, and Associate Professor Dr. Horacio Cabral at Department of Bioengineering, Graduate School of Engineering, the University of Tokyo for allocating the time to review my work even during their busy schedule. The author also like to thank them for their important suggestions and valuable discussion that have augmented the overall value of the thesis.

The author would like to express indebtedness to Japan International Cooperation Agency (JICA) for providing the Ph.D. scholarship through the Future Researchers at

IITH to Enhance Network Development with Scholarship of Japan (FRIENDSHIP) program.

Finally, the author would like to extend his appreciation to the laboratory members and family members for all the support and encouragement.

Majarikar Virendra Jiwanrao

Department of Materials Engineering

Graduate School of Engineering

The University of Tokyo

September, 2019

LIST of WORKS

LIST of papers

1. V. Majarikar, H. Takehara and T. Ichiki. “Microcapillary electrophoresis chip with a bypass channel for autonomous compensation of hydrostatic pressure flow”. Microfluidics and Nanofluidics, 22:110 (2018)

2. V. Majarikar, H. Takehara, and T. Ichiki, “Adsorption phenomena of anionic and cationic nanoliposomes on the surface of poly(dimethylsiloxane) microchannel”. J. Photopolymer Sci. Technol., 32, pp. 107–113 (2019)

LIST of presentations (International conference)

1. V. Majarikar, H. Takehara and T. Ichiki, “Characterization of nanoparticle's surface based on the analysis of electrokinetic phenomena”, 31st International Microprocesses and Nanotechnology Conference (MNC), South Korea (November 2017)

2. Virendra Majarikar, Hiroaki Takehara, Takanori Ichiki, “Adsorption phenomena of nanoliposomes on PDMS microchannel’s surface”, The 66th JSAP Spring Meeting, Tokyo, Japan (March 2019)

LIST of presentations (Domestic conference and symposium)

1. V. Majarikar, H. Takehara and T. Ichiki, “Development of a microfluidic chip for electrophoresis measurement of extracellular vesicles”, 18th University of Tokyo Life Science Symposium, Tokyo (June 2018)

2. V. Majarikar, H. Takehara and T. Ichiki, “Microcapillary electrophoresis chip for characterization of nanoparticles in liquids”, 17th UT2 Workshop (University of Toronto – University of Tokyo), Tokyo (June 2018)